7864 *Inorg. Chem.* **2009**, *48*, 7864–7884
DOI: 10.1021/ic900834z

Inorganic Chemistry
Article

Detailed Spectroscopic, Thermodynamic, and Kinetic Studies on the Protolytic Equilibria of Fe^{III}cydta and the Activation of Hydrogen Peroxide

Ariane Brausam,[†] Joachim Maigut,[†] Roland Meier,[†] Petra Á. Szilágyi,[‡] Hans-Jürgen Buschmann,[§] Werner Massa,[⊥] Zoltán Homonnay,[‡] and Rudi van Eldik*,[†]

[†]*Inorganic Chemistry, Department of Chemistry and Pharmacy, University of Erlangen-Nürnberg, Egerlandstrasse 1, 91058 Erlangen, Germany,* [‡]*Department of Nuclear Chemistry, Eötvös Loránd University, 1117 Budapest, Pázmány P., Hungary,* [§]*Deutsche Textilforschungszentrum Nord-West eV, Institut an der Universität Duisburg-Essen, Adlerstrasse 1, 47798 Krefeld, Germany, and* [⊥]*Fachbereich Chemie, Philipps-Universität Marburg, Hans-Meerwein-Strasse, 35043 Marburg, Germany*

Received April 29, 2009

The crystal structure of the as-yet-unknown salt $K[Fe^{III}(cydta)(H_2O)]\cdot 3H_2O$, where cydta = (±)-*trans*-1,2-cyclohexanediaminetetraacetate, has been resolved: orthorhombic space group *Pbca* with R1 = 0.0309, wR2 = 0.0700, and GOF = 0.99. There are two independent $[Fe^{III}(cydta)(H_2O)]^-$ anions in the asymmetric unit, and the ligand is (*R*,*R*)-cydta in both cases. The coordination polyhedron is a seven-coordinate capped trigonal prism where the quadrilateral face formed by the four ligand donor oxygen atoms is capped by the coordinated water molecule. The speciation of $[Fe^{III}(cydta)(H_2O)]^-$ in water was studied in detail by a combination of techniques: (i) Measurements of the pH dependence of the $Fe^{III/II}$cydta redox potentials by cyclic voltammetry enabled the estimation of the stability constants (0.1 M KNO_3, 25 °C) of $[Fe^{III}(cydta)(H_2O)]^-$ (log $\beta^{III}_{110} = 29.05 \pm 0.01$) and $[Fe^{II}(cydta)(H_2O)]^{2-}$ (log $\beta^{II}_{110} = 17.96 \pm 0.01$) as well as $pK^{III}_{a1OH} = 9.57$ and $pK^{II}_{a1H} = 2.69$. The formation enthalpy of $[Fe^{III}(cydta)(H_2O)]^-$ ($\triangle H^\circ = -23 \pm 1$ kJ mol^{-1}) was measured by direct calorimetry and is compared to the corresponding value for $[Fe^{III}(edta)(H_2O)]^-$ ($\triangle H^\circ = -31 \pm 1$ kJ mol^{-1}). (ii) pH-dependent spectrophotometric titrations of Fe^{III}cydta lead to $pK^{III}_{a1OH} = 9.54 \pm 0.01$ for deprotonation of the coordinated water and a dimerization constant of log $K_d = 1.07$. These data are compared with those of Fe^{III}pdta (pdta = 1,2-propanediaminetetraacetate; $pK^{III}_{a1OH} = 7.70 \pm 0.01$, log $K_d = 2.28$) and Fe^{III}edta ($pK^{III}_{a1OH} = 7.52 \pm 0.01$, log $K_d = 2.64$). Temperature- and pressure-dependent ^{17}O NMR measurements lead to the following kinetic parameters for the water-exchange reaction at $[Fe^{III}(cydta)(H_2O)]^-$ (at 298 K): $k_{ex} = (1.7 \pm 0.2) \times 10^7$ s^{-1}, $\triangle H^{\ddagger} = 40.2 \pm 1.3$ kJ mol^{-1}, $\triangle S^{\ddagger} = +28.4 \pm 4.7$ J mol^{-1} K^{-1}, and $\triangle V^{\ddagger} = +2.3 \pm 0.1$ cm^3 mol^{-1}. A detailed kinetic study of the effect of the buffer, temperature, and pressure on the reaction of hydrogen peroxide with $[Fe^{III}(cydta)(H_2O)]^-$ was performed using stopped-flow techniques. The reaction was found to consist of two steps and resulted in the formation of a purple Fe^{III} side-on-bound peroxo complex $[Fe^{III}(cydta)(\eta^2\text{-}O_2)]^{3-}$. The peroxo complex and its degradation products were characterized using Mössbauer spectroscopy. Formation of the purple peroxo complex is only observable above a pH of 9.5. Both reaction steps are affected by specific and general acid catalysis. Two different buffer systems were used to clarify the role of general acid catalysis in these reactions. Mechanistic descriptions and a comparison between the edta and cydta systems are presented. The first reaction step reveals an element of reversibility, which is evident over the whole studied pH range. The positive volume of activation for the forward reaction and the positive entropy of activation for the backward reaction suggest a dissociative interchange mechanism for the reversible end-on binding of hydrogen peroxide to $[Fe^{III}(cydta)(H_2O)]^-$. Deprotonation of the end-on-bound hydroperoxo complex leads to the formation of a seven-coordinate side-on-bound peroxo complex $[Fe^{III}(cydta)(\eta^2\text{-}O_2)]^{3-}$, where one carboxylate arm is detached. $[Fe^{III}(cydta)(\eta^2\text{-}O_2)]^{3-}$ can be reached by two different pathways, of which one is catalyzed by a base and the other by deprotonated hydrogen peroxide. For both pathways, a small negative volume and entropy of activation was observed, suggesting an associative interchange mechanism for the ring-closure step to the side-on-bound peroxo complex. For the second reaction step, no element of reversibility was found.

Introduction

Nonheme iron(III) complexes are widely used as catalysts in oxidation reactions. Especially, their reactions with hydrogen peroxide as a cheap oxidizing agent have received much attention. Key intermediates formed during these processes are peroxo species $Fe^{III}OO$ and hydroperoxo species $Fe^{III}OOH$, resulting from initial iron(II) dioxygen adducts as the "activated" forms of the catalytic site in many monoiron biomolecules. In a similar way, diiron(II) enzymes tend to

*To whom correspondence should be addressed. E-mail: vaneldik@chemie.uni-erlangen.de.

 Published on Web 07/20/2009

form bridged peroxo $Fe^{III}-O-O-Fe^{III}$ intermediates. These nonheme iron peroxo intermediates have been characterized by various techniques.[1,2] One well-characterized peroxo species is the purple complex $[Fe^{III}(edta)(\eta^2\text{-}O_2)]^{3-}$, formed upon the addition of hydrogen peroxide to $[Fe^{III}(edta)(H_2O)]^-$. This reaction was first studied in 1956[3] and was found to catalyze the oxidation of organic substrates,[4] the polymerization of styrene,[5] and the decomposition of H_2O_2.[6,7] The $[Fe^{III}(edta)(\eta^2\text{-}O_2)]^{3-}$ complex was proven to be a high-spin Fe^{III} side-on peroxo complex by a variety of techniques such as Raman spectroscopy,[8−10] Mössbauer spectroscopy,[11,12] low-temperature absorption spectroscopy, variable-temperature and variable-magnetic-field circular dichroism,[10] and paramagnetic resonance spectroscopy.[10,13] In addition, kinetic information on the activation of H_2O_2 by Fe^{III}edta is available.[3,14−17]

In an earlier study, we reported a detailed mechanism for the formation of the purple peroxo species.[16] With the aid of stopped-flow techniques, we investigated the effect of the buffer, temperature, and pressure on the reaction of hydrogen peroxide with $[Fe^{III}(edta)(H_2O)]^-$. The reaction was found to consist of two reversible steps. The first step was ascribed to the coordination of hydrogen peroxide to $[Fe^{III}(edta)(H_2O)]^-$, leading to an end-on-bound hydroperoxo complex, followed by intramolecular ring closure to form the side-on-bound peroxo complex. Both steps are affected by general acid catalysis.

In order to obtain more information on the reactivity of iron(III) complexes with poly(aminecarboxylate) ligands toward hydrogen peroxide, we have selected $[Fe^{III}(cydta)(H_2O)]^-$ (cydta = *N*,*N*′,*N*″,*N*‴-1,2-cyclohexanediaminetetraacetate) as another representative of this ligand family for the present study. We focused especially on the interpretation of the reactivity and structure differences between Fe^{III}cydta and Fe^{III}edta. These differences become evident by a significant difference between the pK_a values of the coordinated water molecules in $[Fe^{III}(edta)(H_2O)]^-$ and $[Fe^{III}(cydta)(H_2O)]^-$. Furthermore, the differences in complex stability between $[Fe^{III}(cydta)(H_2O)]^-$ and the edta complex was reinvestigated by pH-dependent cyclovoltammetry. A reinvestigation of the pK_{a1OH} values by pH- and concentration-dependent spectrophotometric titrations was necessary because such a determination can only be carried out reliably if the concurrently occurring dimerization equilibrium is appropriately considered.

In addition, the water-exchange reaction of both complexes was reinvestigated using variable-temperature and variable-pressure ^{17}O NMR techniques. In order to obtain more accurate values for the activation parameters ($\Delta H^{\ddagger}$, $\Delta S^{\ddagger}$, and $\Delta V^{\ddagger}$), not only line broadening but also the shift of the ^{17}O signal was taken into account.

In our earlier study of the reaction of hydrogen peroxide with $[Fe^{III}(edta)(H_2O)]^-$, it was observed that the reaction depends strongly on the pH and buffer concentration used, and therefore we again employed different buffers to establish the role of general acid catalysis in the reaction of $[Fe^{III}(cydta)(H_2O)]^-$ with H_2O_2. The effect of the temperature and pressure on the observed kinetics was studied in detail, and the activation parameters ($\Delta H^{\ddagger}$, $\Delta S^{\ddagger}$, and $\Delta V^{\ddagger}$) are reported. The different Fe^{III}cydta species in solution, viz., aqua, hydroxo, and dimeric species, as well as the purple species formed upon reaction with hydrogen peroxide, were all characterized by Mössbauer spectroscopy. It turned out that the peroxo species formed in the Fe^{III}cydta system showed properties quite similar to those found for the Fe^{III}edta system. From a combination of all of these data, a comprehensive characterization of the Fe^{III}cydta solution behavior including its reaction product with hydrogen peroxide was possible. On the basis of a detailed comparison with Fe^{III}edta, the mechanistic similarities and differences for the activation of hydrogen peroxide by Fe^{III}edta and Fe^{III}cydta can be presented in a straightforward manner.

Experimental Section

Synthesis of K[Fe(cydta)(H$_2$O)]·3H$_2$O. A total of 3.64 g (0.01 mol) of H_4cydta and 4.62 g (0.01 mol) of $FeClO_4 \cdot 6H_2O$ were suspended in 20 mL of distilled water and heated on a stirring plate until the solution became clear yellow-brown. The careful addition of 4.0 g (0.04 mol) of $KHCO_3$ led to a clear, reddish-brown solution with a pH of 6−7. After cooling to room temperature, acetone was added to the aqueous solution until the first turbidity was observed. The solution was then placed in a refrigerator at 5 °C and dark-yellow-brown crystals began to form. Crystallization was complete after 2 days. The dark-yellow-brown crystals were separated by filtration and air-dried.

Typical yield: 4 g (78.5%). Anal. Calcd for $C_{14}H_{26}FeKN_2O_{12}$ (509.32 g mol^{-1}): C, 33.02; H, 5.15; N, 5.50. Found: C, 33.00; H, 5.20; N, 5.54.

Crystals suitable for X-ray diffraction were prepared as follows: 1 g of the previously prepared yellow-brown material was dissolved in a minimum amount of water on a stirring plate. The clear solution was gently layered with an equivalent volume of acetone in a larger reagent glass. The mixture, which appeared as two separated phases, was covered with Parafilm and left to stand at room temperature for several days. With time, brown single crystals grew at the boundary layer between the solution phases. These were removed manually and subjected to X-ray diffraction. The crystal structure has been deposited at the Cambridge Crystallographic Data Center under the number CCDC 729487.

(1) Girerd, J.-J.; Banse, F.; Simaan, A. J. *Struct. Bonding (Berlin)* **2000**, *97*, 145–177.
(2) (a) Rohde, J.-U.; Bukowski, M. R.; Que, L. *Curr. Opin. Chem. Biol.* **2003**, *7*, 674–682. (b) Zhang, X.; Furutach, H.; Fujinami, S.; Nagatomo, S.; Maeda, Y.; Watanabe, Y.; Kitagawa, T.; Suzuki, M. *J. Am. Chem. Soc.* **2005**, *127*, 826–827. (c) Katona, G.; Carpentier, P.; Vincent, N.; Amara, P.; Adam, V.; Ohana, J.; Tsanov, N.; Bourgeois, D. *Science* **2007**, *316*, 449–453. (d) Martinho, M.; Dorlet, P.; Riviere, E.; Thibon, A.; Ribal, C.; Banse, F.; Girerd, J. J. *Chem.—Eur. J.* **2008**, *14*, 3182–3188.
(3) Cheng, K. L.; Lott, P. F. *Anal. Chem.* **1956**, *28*, 462–465.
(4) Walling, C.; Kurz, M.; Schugar, H. J. *Inorg. Chem.* **1970**, *9*, 931–937.
(5) Bond, J.; Brown, C. W.; Rushton, G. S. *J. Polym. Sci.* **1964**, *2*, 1015–1017.
(6) Kachanova, Z. P.; Kudryavtseva, E. L.; Purmalis, A. *Zh. Fiz. Khim.* **1974**, *48*, 1449–1453.
(7) Kachanova, Z. P.; Purmal, A. P. *Zh. Fiz. Khim.* **1964**, *38*, 2506–2508.
(8) Ahmad, S.; McCallum, J. D.; Shiemke, A. K.; Appelman, E. H.; Loehr, T. M.; Sanders-Loehr, J. *Inorg. Chem.* **1988**, *27*, 2230–2233.
(9) Hester, R. E.; Nour, E. M. *J. Raman Spectrosc.* **1981**, *11*, 35–38.
(10) Neese, F.; Solomon, E. I. *J. Am. Chem. Soc.* **1998**, *120*, 12829–12848.
(11) Sharma, V. K.; Szilagyi, P. A.; Homonnay, Z.; Kuzmann, E.; Vertes, A. *Eur. J. Inorg. Chem.* **2005**, 4393–4400.
(12) Horner, O.; Jeandey, C.; Oddou, J.-L.; Bonville, P.; Latour, J.-M. *Eur. J. Inorg. Chem.* **2002**, 1186–1189.
(13) Fujii, S.; Tsueda, C.; Yamabe, K.; Nakajima, K.; Sakai, H. *Inorg. Chim. Acta* **2008**, *361*, 1207–1211.
(14) Bull, C.; McClune, G. J.; Fee, J. A. *J. Am. Chem. Soc.* **1983**, *105*, 5290–5300.
(15) Francis, K. C.; Cummins, D.; Oakes, J. *J. Chem. Soc., Dalton Trans.* **1985**, 493–501.
(16) Brausam, A.; van Eldik, R. *Inorg. Chem.* **2004**, *43*, 5351–5359.
(17) Sharma, V. K.; Millero, F. J.; Homonnay, Z. *Inorg. Chim. Acta* **2004**, *357*, 3583–3587.

Preparation of Solutions for Mössbauer Measurements. Preparation of a $^{57}Fe^{III}$cydta Stock Solution. A total of 0.27 g (7.3 mmol) of cydta monohydrate was suspended in 5 mL of H_2O, and a concentrated NaOH solution was added dropwise until a clear solution was obtained. A total of 0.0139 g (0.2 mmol) of ^{57}Fe (95.95% enriched) dissolved in 5 mL of HNO_3 (ca. 12%) was added dropwise to the cydta solution. A yellow solution was obtained, and the pH was adjusted to 5 with a concentrated NaOH solution. The total concentration of iron(III) was about 0.021 M.

Preparation of $[^{57}Fe^{III}(edta)(\eta^2\text{-}O_2)]^{3-}$ Solutions. The desired pH of a stock solution was adjusted with concentrated NaOH. The addition of an excess of hydrogen peroxide resulted in the formation of the purple peroxo complex. To slow down the degradation reaction of the peroxo complex, the solution was cooled to about 0 °C in an ice bath. The resulting solution was quickly frozen drop by drop on an aluminum slab soaked in liquid nitrogen. The contact of the liquid drops of the solution with the aluminum metal at 80 K provided a cooling rate that promptly quenched the reaction, and the structure of the chemical species in the liquid state was preserved.[18] The frozen droplets were placed in a sample holder and mounted in a cryostat. The Mössbauer spectra were recorded at ~83 K. All isomer shifts are given relative to α-Fe at room temperature. The spectra were evaluated with the Mösswinn code.

Preparation of Solutions for Kinetic Measurements. Solutions of $[Fe^{III}(cydta)(H_2O)]^-$ were prepared from solid $K[Fe^{III}(cydta)(H_2O)]\cdot 3H_2O$. In all solutions, an equimolar concentration of H_4cydta (Acros Organics) was present to prevent precipitation of iron hydroxide at higher pH. $NaClO_4$ (Aldrich) was used to adjust the ionic strength to 0.5 M. The employed buffers, viz., 3-(cyclohexylamino)propansulfonic acid (CAPS) and glycine, were purchased from Roth. NaOH (Acros Organics) was used to adjust the pH of the buffer solutions. Solutions of H_2O_2 were prepared by dilution of a 35% stock solution of H_2O_2 (Acros Organics). To verify the concentration of the H_2O_2 stock solution, kinetic measurements were repeated regularly at a fixed H_2O_2 concentration throughout the study. No changes in the values of the rate constants were observed, from which it could be concluded that the concentration of H_2O_2 remained constant throughout the measurements. All chemicals were of the highest quality commercially available and used without further purification. All solutions were prepared with deionized water.

pH measurements were performed on a Metrohm 632 pH meter equipped with a Mettler Toledo InLab 422 glass electrode, which was filled with NaCl instead of KCl to prevent precipitation of $KClO_4$. UV/vis spectra were recorded on a Cary 5G UV/vis/near-IR spectrophotometer. Kinetic measurements were performed with a thermostatted (±0.1 °C) SX-18 MV Applied Photophysics stopped-flow spectrometer. Absorbance changes were recorded at 360 and 545 nm. Stopped-flow experiments at pressures up to 170 MPa were performed on a custom-built instrument described before.[19,20] Kinetic traces were recorded on an IBM-compatible computer and analyzed with the OLIS KINFIT (Bogart, GA) set of programs. All kinetic measurements were performed under pseudo-first-order conditions; i.e., at least a 10-fold excess of hydrogen peroxide was employed. Reported rate constants are the mean values from at least five kinetic runs.

Pressure- and Temperature-Dependent ^{17}O NMR for Water Exchange on $[Fe^{III}(cydta)(H_2O)]^-$. Materials. The reagents used in the investigation of the water-exchange reaction were all of analytical-grade quality. The edta and cydta ligands (Acros Organics) were used as delivered without further purification. The solutions were prepared in doubly distilled water. The ionic strength was adjusted with $NaClO_4$ (Merck) to I = 0.5 M. The samples for the water-exchange measurements were prepared by dissolving the ligand in a 0.1 M sodium acetate buffer solution. The pH was measured with a Metrohm 713 pH meter using a Metrohm glass electrode (filled with sodium chloride instead of potassium chloride to prevent precipitation of poorly soluble potassium perchlorate) and adjusted to 5.0 with NaOH (Acros Organics). The appropriate amount of $Fe(NO_3)_3$ (Acros Organics) was added to give a total complex concentration of 20 mM. The complex solution was enriched with the NMR-active ^{17}O isotope by the addition of $H_2{}^{17}O$ (10%, Deutero), leading to a total enrichment of 1% for the solution in the NMR tube.

Measurements. The ^{17}O NMR spectra were recorded on a Bruker AVANCE DRX 400WB spectrometer operating at a resonance frequency of 54.24 MHz at 9.4 T. The measurements at atmospheric pressure were performed with a commercial 5 mm Bruker broad-band probe thermostatted with a Bruker B-VT 3000 variable-temperature unit. To estimate the shift of the ^{17}O NMR resonance, the samples were sealed in spherical NMR glasses to avoid susceptibility corrections of the measured data. Pressure-dependent measurements were carried out with a homemade thermostatted high-pressure probe.[21] The sample was measured in a standard 5 mm NMR tube cut to a length of 50 mm. For transmittance of the pressure to the solution, the NMR tube was closed with a moveable macor piston. Details describing the various kinetic features of the water-exchange reaction are summarized in the Supporting Information.

$E_{1/2}$ Measurements as a Function of the pH. $E_{1/2}$ values were measured cyclovoltammetrically (CV). Cyclic voltammograms were recorded for gold disk (Metrohm) or hanging mercury drop electrode (HMDE; model CGME 900, BAS) working electrodes interfaced to a BAS 100W analyzer. Reproducible cyclic voltammograms were obtained with the gold disk by applying a combination of polishing and electrochemical activation of the gold surface. The electrochemical cell was thermostatted at 25.0 ± 0.2 °C during the measurement. Potentials were measured versus a saturated calomel electrode (SCE).

pH-Dependent UV/vis Measurements. Sample solutions for the pH-dependent UV/vis measurements were prepared from standard solutions that contained precise amounts of $K[Fe(cydta)(H_2O)]\cdot 3H_2O$. pH-dependent spectrophotometric titrations were carried out with a Varian CARY 1 UV/vis spectrophotometer fitted with a thermostatted sample holder. All measurements were carried out at 25.0 ± 0.1 °C in 0.1 M KNO_3 in an optical cell with d = 0.01 mm.

Results and Discussion

1. Structural Features of $[Fe^{III}(cydta)(H_2O)]^-$ in the Solid State. We were able to obtain a further crystal structure of a $[Fe^{III}(cydta)(H_2O)]^-$ salt and were successful at obtaining single crystals of the so-far-unknown potassium salt, $K[Fe(cydta)(H_2O)]\cdot 3H_2O$ (**1**). This was done to see if there would be significant changes at the iron(III) coordination polyhedron, as compared to the $FeN_2O_4O_W$ moieties found before in the corresponding calcium[22] and sodium salts of the complex.[23]

Cohen and Hoard published a detailed study on the calcium salt[22] of $[Fe^{III}(cydta)(H_2O)]^-$, whereas Seibig and van Eldik investigated the structure of

(18) Vertes, A., Nagy, D. L., Eds. *Moessbauer Spectroscopy of Frozen Solutions*; Akadémiai Kiadó, Budapest, 1990; p 303.
(19) van Eldik, R.; Palmer, D. A.; Schmidt, R.; Kelm, H. *Inorg. Chim. Acta* **1981**, *50*, 131–135.
(20) van Eldik, R.; Gaede, W.; Wieland, S.; Kraft, J.; Spitzer, M.; Palmer, D. A. *Rev. Sci. Instrum.* **1993**, *64*, 1355–1357.
(21) Zahl, A.; Neubrand, A.; Aygen, S.; van Eldik, R. *Rev. Sci. Instrum.* **1994**, *65*, 882–886.
(22) Cohen, G. H.; Hoard, J. L. *J. Am. Chem. Soc.* **1966**, *88*, 3228–3234.
(23) Seibig, S.; van Eldik, R. *Inorg. Chim. Acta* **1998**, *279*, 37–43.

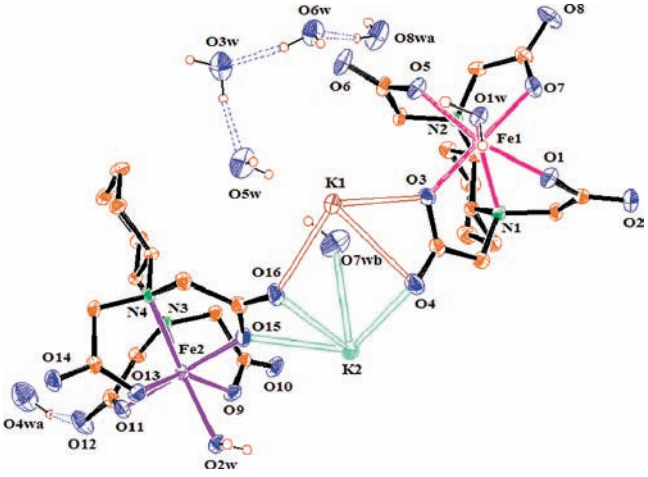

Figure 1. Asymmetric unit in the crystals of **1** that reflects the presence of two crystallographically unique $[Fe(cydta)(H_2O)]^-$ anions (**Fe1**, iron-donor atom interactions in pink; **Fe2**, iron-donor atom interactions in violet). Crystal water molecules O4w, O7w, and O8w are disordered over two positions, and only the higher occupied one is shown, i.e., **O4wa** [occupation factor **0.637(3)** vs **0.363(3)** for O4wb], **O7wb** [0.881(15) in favor of 0.119(15) for O7wA], and **O8wa** [0.689(7) vs 0.311(7) for O8wb].

$Na[Fe^{III}(cydta)(H_2O)]\cdot 5H_2O$.[23] The major difference from the structurally more explored $[Fe^{III}(edta)(H_2O)]^-$ complex anion[24−26] is that the different stereochemistries of the chelates (i.e., edta vs cydta) lead to an altered complex geometry for the cydta complexes. A capped-trigonal prismatic arrangement[27] was observed for $[Fe^{III}(cydta)(H_2O)]^-$ salts instead of the well-known pentagonal-bipyramidal coordination polyhedron in the case of the Fe^{III}edta complexes.[24−26] We have recently reported a detailed description of the stereochemical peculiarities of six- and seven-coordinate cydta complexes,[28] such that we focus here on the peculiarities found in **1** as compared to the related calcium and sodium salts. Basic crystallographic data for the structural estimation of **1** are collected in Table S1 (Supporting Information). The asymmetric unit of **1** is shown in Figure 1, from which it becomes evident that two crystallographically unique $[Fe(cydta)(H_2O)]^-$ anions are present. The comparison of both complex structures in the upper part of Table 1 reveals, furthermore, that chiralities are identical in both cases and can be assigned to the Λ ($\lambda_E\lambda\lambda\lambda\lambda$) isomer with (*R*,*R*)-cydta as the chelate. As a result of the orthorhombic space group *Pbca*, the Δ ($\delta_E\delta\delta\delta\delta$) isomer with (*S*,*S*)-cydta is present in the crystal with a fraction of 50%.

There is a very close agreement between all (Fe−L) distances with one exception, which is the ($Fe-O_W$) bond length. In the latter case, the average value between complex anions **Fe1** and **Fe2** [$(Fe-O_W)_{av}$ = 2.1409(2) Å] exceeds the iron−water bond lengths in the other two structures by ∼0.04 Å, which is a significant elongation. What are the factors responsible for this difference? During our studies to elucidate the interdependencies between solid and solution structures of iron(III) complexes with aminopolycarboxylate chelates, it turned out that hydrogen bonds formed by the Fe^{III}-coordinated water molecules are the critical factor that controls the $Fe-OH_2$ distance in the solid state.[25,29−31]

The bond-length data collected in Table 1 show a comparison between the Fe−L distances found in **1** and those estimated for $Ca[Fe^{III}(cydta)(H_2O)]_2\cdot 8H_2O$[22] and $Na[Fe^{III}(cydta)(H_2O)]\cdot 5H_2O$.[23]

The correlation in Figure 2 reveals the following. The more intense the electrostatic interactions are along the appropriate O−H···A contacts, the shorter is the particular $Fe^{III}-OH_2$ bond. In general, the strength of the hydrogen-bonding interaction can be regarded as the major factor governing the $M-OH_2$ bond distance in crystals of a $[M(L)(H_2O)]$ complex. The stronger the hydrogen bonds of the protons bound to the metal-coordinated water oxygen with appropriate adjacent acceptor atoms, the shorter is the $M-OH_2$ bond length. Acceptor A in the M−(H)O−H···A arrangement electrostatically attracts the single hydrogen atom largely as a positively charged proton H^+, leaving a considerable amount of negative charge density on the water oxygen atom. Because there are two hydrogen-bonding interactions, the nature of the water oxygen as a donor atom partially approaches that of a coordinated hydroxo donor OH^-.

The different patterns of hydrogen bonding in **1** as compared to those in the calcium and sodium salts of the $[Fe^{III}(cydta)(H_2O)]^-$ anion are mainly caused by different packing patterns in the various crystals. As discussed below in conjunction with the water-exchange kinetics of Fe^{III}cydta, the solid-state structure of **1** is presumably closer related to the aqueous solution structure of $[Fe^{III}(cydta)(H_2O)]^-$ than structures of the corresponding calcium and sodium salts. This difference in packing patterns between the three $[Fe^{III}(cydta)(H_2O)]^-$ structures is illustrated in Figures S1−S4 and Table S2 (Supporting Information).

2. Complex-Formation and Protolytic Equilibria of Fe^{III} with cydta. 2.1. Estimation of Thermodynamic Parameters for the Complex Formation of $[Fe^{III}(cydta)(H_2O)]^-$ and $[Fe^{II}(cydta)(H_2O)]^{2-}$. 2.1.1. Complex Stabilities from pH-dependent Redox Potential Data. Evaluation via EFIT. The stability parameters for the complex formation of ferrous[34] and ferric ions[35−37] with cydta have been studied several times [equilibria (1a) and (1b)]. The same is true for estimation of the magnitude of the protolytic constants for

(24) Lind, M. D.; Hoard, J. L. *Inorg. Chem.* **1964**, *3*, 34–43.
(25) Meier, R.; Heinemann, F. W. *Inorg. Chim. Acta* **2002**, *337*, 317–327.
(26) Solans, X.; Font Altaba, M.; Garcia-Oricain, J. *Acta Crystallogr., Sect. C: Cryst. Struct. Commun.* **1984**, *C40*, 635–638.
(27) Maigut, J.; Meier, R.; Zahl, A.; van Eldik, R. *Inorg. Chem. Commun.* **2008**, *47*, 5702–5719.
(28) Porai-Koshits, M. A.; Pozhidaev, A. I.; Polynova, T. N. *Zh. Strukt. Khim.* **1974**, *15*, 1117–1126.
(29) Meier, R.; Maigut, J.; Kallies, B.; Lehnert, N.; Paulat, F.; Heinemann, F. W.; Zahn, G.; Feth, M. P.; Krautscheid, H.; Van Eldik, R. *Chem. Commun.* **2007**, 3960–3962.
(30) Meier, R.; Molinier, M.; Anson, C.; Powell Anne, K.; Kallies, B.; van Eldik, R. *Dalton Trans.* **2006**, 5506–5514.
(31) Meier, R.; Bedell, S. A.; Henkel, G. *Inorg. Chim. Acta* **2002**, *337*, 337–343.
(32) Weakliem, H. A.; Hoard, J. L. *J. Am. Chem. Soc.* **1959**, *81*, 549–555.
(33) Crane, J. D.; Sharp, K. *Inorg. Chem. Commun.* **2003**, *7*, 107–110.
(34) Bond, J.; Jones, T. I. *Trans. Faraday Soc.* **1959**, *55*, 1310–1318.
(35) Bottari, E.; Anderegg, G. *Helv. Chim. Acta* **1967**, *50*, 2349–2356.
(36) Woodruff, W. H.; Margerum, D. W. *Inorg. Chem.* **1974**, *13*, 2578–2585.
(37) Ahmad, J. A. M.; Higginson, W. C. E. *J. Chem. Soc., Dalton Trans.* **1983**, 1449–1459.

Table 1. Comparison of the Fe^{III}-Donor Atom Bond Lengths Found for **1** with the Corresponding Distances[a] and the Related Distances in $Ca[Fe(cdta)(H_2O)]_2 \cdot 8H_2O$ and $Na[Fe(cydta)(H_2O)] \cdot 5H_2O$

(a) Corresponding Distances

	$K[Fe(cydta)(H_2O)] \cdot 3H_2O$ (**1**)			
N_1	Fe1−N1	2.3169(14)	Fe2−N3	**2.2545(13)**
N_2	Fe1−N2	2.2728(13)	Fe2−N4	**2.3265(14)**
O_{G1}	Fe1−O1	2.0961(12)	Fe2−O9	2.0718(12)
O_{G2}	Fe1−O5	2.0739(12)	Fe2−O13	2.1027(12)
O_W	Fe1−O1W	**2.1411(12)**	Fe2−O2W	**2.1409(12)**
O_{R1}	Fe1−O3	1.9734(13)	Fe2−O11	2.0185(13)
O_{R2}	Fe1−O7	2.0108(13)	Fe2−O15	1.9890(13)

	$Ca[Fe(cdta)(H_2O)]_2 \cdot 8H_2O$ (*CACHAF10*)	$Na[Fe(cydta)(H_2O)] \cdot 5H_2O$ (*PUHNOV*)
N_1	2.299(4)	2.291(6)
N_2	2.282(4)	2.288(6)
O_{G1}	2.097(4)	2.062(5)
O_{G2}	2.088(4)	2.094(5)
O_W	2.092(3)	2.106(5)
O_{R1}	2.035(4)	2.005(6)
O_{R2}	2.001(4)	2.020(6)

(b) Related Distances

	1	$Ca[Fe(cdta)(H_2O)]_2 \cdot 8H_2O$ (*CACHAF10*)	$Na[Fe(cydta)(H_2O)] \cdot 5H_2O$ (*PUHNOV*)
$(Fe-N)_{av}$	2.29(3)	2.29(1)	2.290(2)
$(Fe-OG)_{av}$	2.09(2)	2.09(1)	2.08(2)
$(Fe-OR)_{av}$	2.00(2)	2.02(2)	2.01(1)
$Fe-O_W$	2.1409(2)	2.092	2.106
$(Fe-O_{all})_{av}$	2.06(6)	2.06(4)	2.06(4)

[a] The indices G and R were those introduced by Hoard[32] for more (G = in-plane) and less (R = out-of-plane) strained chelate rings.

Fe^{II}cydta[37] and Fe^{III}cydta.[38,39] The purpose of these measurements was to estimate the stability constant of $[Fe^{III}(cydta)(H_2O)]^-$ at 25 °C and 0.1 M KNO_3 in order to obtain a reliable estimate of $\Delta G°$ under these conditions. This, in turn, should enable, along with a value for the complex-formation enthalpy, $\Delta H°$, the evaluation of the complex-formation entropy, $\Delta S°$.

$$[Fe^{II}(H_2O)_6]^{2+} + cydta^{4-} \overset{\beta^{II}_{110}}{\rightleftharpoons} [Fe^{II}(cydta)(H_2O)]^{2-} + 5H_2O \quad (1a)$$

$$[Fe^{III}(H_2O)_6]^{3+} + cydta^{4-} \overset{\beta^{II}_{110}}{\rightleftharpoons} [Fe^{III}(cydta)(H_2O)]^{-} + 5H_2O \quad (1b)$$

It was our intention to estimate these data as precisely as possible to obtain a benchmark value for comparison with that of $[Fe^{III}(edta)(H_2O)]^-$. The $\Delta H°$ value for the complex formation of Fe^{III}edta has been measured only once[40] and shows a large discrepancy with the $\Delta H°$ value

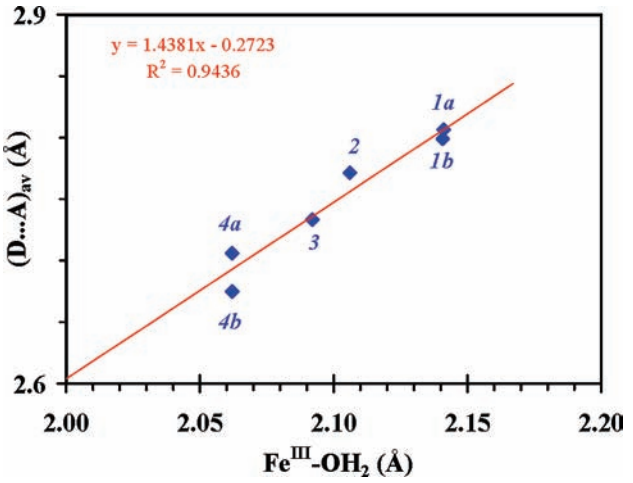

Figure 2. Correlation between the $Fe^{III}-OH_2$ bond distances in various salt structures of $[Fe^{III}(cydta)(H_2O)]^-$ and the averaged donor−acceptor distances of both the water proton hydrogen-bonding interactions of type O−H···A where D = O. Values indicated as **1a**, **1b**, **2**, and **3** as well as **4a** and **4b** belong to structures **1**, $Na[Fe(cydta)(H_2O)] \cdot 5H_2O$, $Ca[Fe(cdta)(H_2O)]_2 \cdot 8H_2O$, and a closely related amide structure[33].

estimated in the current work for the formation of Fe^{III}edta (see Table 4).[41] It was therefore hoped that a systematic comparison of the thermodynamic features for the formation of $[Fe^{III}(cydta)(H_2O)]^-$ and $[Fe^{III}(edta)(H_2O)]^-$ can help to clarify these uncertainties.

Another goal was the concurrent evaluation of stability and protolytic constants for both Fe^{III}- and Fe^{II}cydta from the same $E_{1/2}$−pH curve to come up with another example to demonstrate the validity of our evaluation software EFIT.[42] The latter has so far been applied successfully for the study of the pH-dependent complex-formation and protolytic constants of various transition-metal complex redox couples.[30,43−45] The basic approach of EFIT is analogous to that applied by Schwarzenbach and Heller for evaluation of the stability and protonation constant data for $Fe^{III/II}$edta,[46] with the difference that a digitalized nonlinear least-squares routine (the Marquardt algorithm) was applied for data evaluation and the pH-dependent redox potentials were not measured by potentiometry but by cyclic voltammetry instead.[42]

As becomes visible from Figure 3, the $Fe^{III/II}$cydta electrode reaction (eq 2a) is highly reversible at a HMDE working electrode because the separation between cathodic and anodic peak potentials, ΔE_p, is still close to 60 mV even at $v \sim 300$ V/s. Also, the ratio of anodic-to-cathodic peak currents (i_{pa}/i_{pc}) remains the same at all applied sweep rates, which indicates complete chemical reversibility[47] of the redox process on the electrode surface. These features do not change when the pH is decreased to the region of pH 2 or increased

(38) Gustafson, R. L.; Martell, A. E. *J. Phys. Chem.* **1963**, *67*, 576–582.
(39) Wilkins, R. G.; Yelin, R. E. *Inorg. Chem.* **1969**, *8*, 1470–1473.
(40) Doi, K. *Talanta* **1978**, *25*, 97–101.
(41) Meier, R. Habilitation Thesis, University of Leipzig, Leipzig, Germany, **2003**.
(42) Meier, R. *EFIT—A General Program for Evaluation of Metal Complex Equilibrium Constants from Redox Potential Data*; University of Leipzig: Leipzig, Germany, **1999**.
(43) Meier, R.; Boddin, M.; Mitzenheim, S.; Kanamori, K. *Met. Ions Biol. Syst.* **1995**, *31*, 45–88.
(44) Meier, R.; Boddin, M.; Mitzenheim, S. In *Bioinorganic Chemistry: Transition Metals in Biology and their Coordination Chemistry*; Trautwein, A. X., Ed.; Wiley-VCH: Weinheim, Germany, 1997; pp 69−77.
(45) Sarauli, D.; Meier, R.; Liu, G.-F.; Ivanovic-Burmazovic, I.; van Eldik, R. *Inorg. Chem.* **2005**, *44*, 7624–7633.
(46) Schwarzenbach, G.; Heller, J. *Helv. Chim. Acta* **1951**, *34*, 1889–1900.
(47) Bard, A. J.; Faulkner, L. R. *Electrochemical Methods—Fundamentals and Applications*; John Wiley & Sons: New York, 1980.

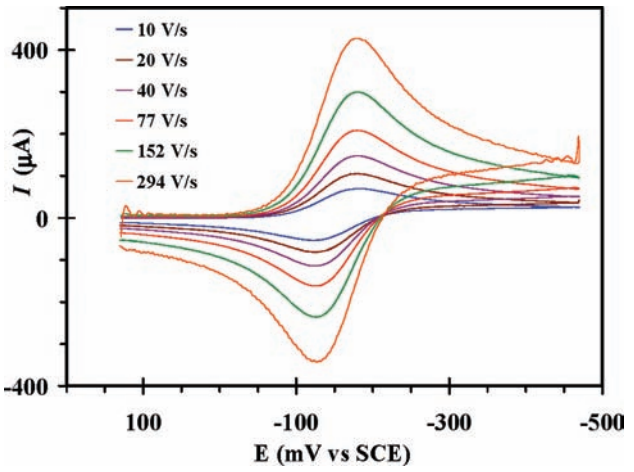

Figure 3. CV of $[Fe^{III/II}(cydta)(H_2O)]^{-/2-}$ in 1 M KNO_3 (pH 6.0) at 25 °C at a HMDE working electrode.

up to pH 11.5 (cf. Figure 4). The pH dependence of $E_{1/2}$, as reflected by the shift of the CVs in Figure 4a, leads to the plot in Figure 4b, where all measured $E_{1/2}$–pH data points (52) are shown together with a fit to these data (solid line) performed by EFIT.

$$[Fe^{III}(cydta)(H_2O)]^- + e^- \overset{E_{1/2c}}{\rightleftharpoons} [Fe^{II}(cydta)(H_2O)]^{2-} \quad (2a)$$

$$[Fe^{III}(H_2O)_6]^{3+} + e^- \overset{E_{1/2aq}}{\rightleftharpoons} [Fe^{II}(H_2O)_6]^{2+} \quad (2b)$$

Taking into account equilibria (1a) and (1b), the relationship between $E_{1/2c}$ and $E_{1/2aq}$ can be expressed as in eq 2c.

$$E_{1/2c} = E_{1/2aq} - RT/nF(\ln \beta^{II}{}_{110}/\ln \beta^{II}{}_{110}) \quad (2c)$$

Basically, the $E_{1/2}$–pH plot in Figure 4b consists of four segments indicated as a–d. In segment a ($1.70 < pH < 2.10$), the slope of the line is −194.5 mV/pH, in agreement with electrode reaction (3a). The slope in segment b (pH 2.10–2.70) is −52.5 mV, thus reflecting the operation of electrode reaction (3b). Between pH 4 and 9, the redox potentials are independent of the pH such that eq 2a describes the appropriate electrode reaction.

$$[Fe^{III}(cydta)(H_2O)]^- + 5H_2O + 3H^+ + e^- \rightleftharpoons [Fe^{II}(H_2O)_6]^{2+} + [H_3cydta]^- \quad (3a)$$

$$[Fe^{III}(cydta)(H_2O)]^- + H^+ + e^- \rightleftharpoons [Fe^{II}(Hcydta)(H_2O)]^- \quad (3b)$$

$$[Fe^{III}(cydta)(OH)]^{2-} + H^+ + e^- \rightleftharpoons [Fe^{II}(cydta)(H_2O)]^{2-} \quad (3c)$$

Between pH 10 and 11.4, $E_{1/2}$ is shifted by −53.3 mV/pH, and the electrode process is expressed by reaction (3c). The pH-independent half-wave potential of the $Fe^{III/II}$cydta redox couple is 18 mV more negative than that of $Fe^{III/II}$edta (first entry in Table 2), leading to a somewhat higher degree of stabilization of the oxidized form over the reduced form in the case of $Fe^{III/II}$cydta as compared to $Fe^{III/II}$edta (cf. the third line in Table 2). The $E_{1/2}$–pH dependence of the $Fe^{III/II}$cydta electrode reaction was eventually evaluated by application of EFIT, and the equilibrium data obtained in this way are compared in Table 2 with those for $Fe^{III/II}$edta measured in a related study.[41]

The $E_{1/2}$ values recorded at 52 different pH values at a metal-to-ligand ratio of 1:5 were inserted into the input matrix of EFIT. Before a suitable fit of the experimental data could be obtained, the mass balance of the appropriate equilibrium system had to be expressed in a proper way. For both the formation of iron(III) and iron(II) complex species, the general equation (4) was applied to introduce the various variables into the EFIT input matrix.

$$\beta_{pqr} = \frac{[Fe_pL_qH_r]}{[Fe_{aq}]^p[L^{n-}]^q[H^+]^r} \quad (4)$$

The following constants, applied as fixed parameters, are also required as EFIT input values: The $E_{1/2aq}$ value of $[Fe(H_2O)_6]^{3+/2+}$ (504.6 mV vs SCE)[41] and six ligand pK_a values ($pK_{a1} = 12.30$, $pK_{a2} = 6.12$, $pK_{a3} = 3.49$, $pK_{a4} = 2.40$, $pK_{a5} = 1.60$, and $pK_{a6} = 0.00$ valid at 25 °C and $I = 0.1$ M KNO_3)[48] were used in the evaluation process. A comparison of the Fe^{III}- and Fe^{II}cydta stability constants estimated in the present work with those listed in the NIST database[48] (cf. Table 2) reveals that our parameters are 1 order of magnitude lower than those in the database. The compilation in Table 3, however, demonstrates that our data compare well with those from previous measurements.

2.1.2. Estimation of the Complex-Formation Enthalpy of $[Fe^{III}(cydta)(H_2O)]^-$. Finally, trials were undertaken to estimate the reaction enthalpy for complex formation of $[Fe^{III}(cydta)(H_2O)]^-$ according to reaction (1c) (cf. above). These measurements were done calorimetrically, and appropriate thermometric titrations were carried out.

$$[Fe^{III}(H_2O)_6]^{3+} + [cydta]^{4-} \overset{\Delta H°}{\rightleftharpoons} [Fe^{III}(cydta)(H_2O)]^- + 5H_2O \quad (1c)$$

The obtained $\Delta H°$ value is compared in Table 4 with related data from the literature and our own data measured for the complex-formation enthalpy of Fe^{III}edta. Our $\Delta H°$ and $\Delta S°$ data for Fe^{III}cydta are in good agreement with those reported by Woodruff and Margerum[36] when slightly different experimental conditions and different methods are taken into account. A large discrepancy is apparent upon comparison of our $\Delta H°$

(48) *NIST Standard Reference Database 46, NIST Critical Stability Constants and Related Thermodynamic Constants of Metal Complexes*, version 7.0; National Institute of Standards and Technology: Gaithersburg, MD, 2003.

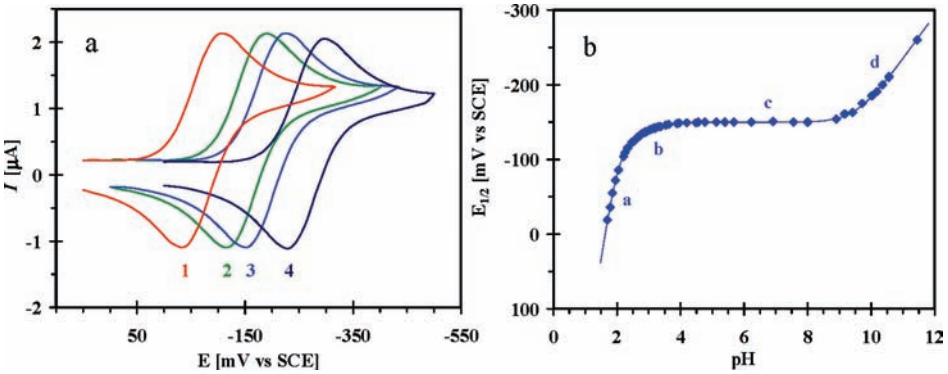

Figure 4. (a) pH dependence of $E_{1/2}$ measured with CV for $Fe^{III/II}$cydta. HMDE, $v = 10$ mV s^{-1}. 0.1 M KNO_3, 25 °C, $[Fe]_T$:$[cydta]_T$ = 1:5 (mM), **1**, pH 2.0, **2**, pH 6.0, **3**, pH 10.0, **4**, pH 11.4. (b) pH dependence of $E_{1/2}$ measured with CV for $Fe^{III/II}$cydta at 25 °C, 0.1 M KNO_3: (blue ◆) 52 values measured at $[Fe]_T$:$[cydta]_T$ = 1:5 between pH 1.70 and 11.47; (blue line) computed using EFIT.

Table 2. Comparison of the Equilibrium Constants of $Fe^{III/II}$edta and $Fe^{III/II}$cydta As Estimated from $E_{1/2}$–pH Measurements (0.1 M KNO_3, 25 °C) Followed by Evaluation with EFIT (Literature Reference Values in *Italics*)[a]

	$Fe^{III/II}$cydta	$Fe^{III/II}$edta[41]
$E_{1/2c}$ [mV vs SCE]	−150.5	−132.5
$\Delta(E_{1/2c} - E_{1/2aq})$ [mV]	655	637.1
$\Delta[\log(\beta^{III}_{110} - \beta^{II}_{110})]$	11.09	10.77
$\log \beta^{III}_{110}$	**29.05 ± 0.01** (*30.0*)[48]	**24.95 ± 0.01** (*25.1*)[48]
$\log \beta^{III}_{11-1}$	19.48 ± 0.03	17.35 ± 0.05
pK^{III}_{a1OH}	9.57	7.60
$\log \beta^{II}_{110}$	**17.96 ± 0.01** (*18.9*)[48]	**14.16 ± 0.01** (*14.3*)[48]
$\log \beta^{II}_{111}$	20.65 ± 0.02	17.07 ± 0.06
pK^{II}_{a1H}	2.69	2.90

[a] $E_{1/2aq}([Fe(H_2O)_6]^{3+/2+}) = 504.6$ mV vs SCE.[41]

Table 3. Comparison of the Stability Constants of $[Fe^{III}(cydta)(H_2O)]^-$ and $[Fe^{II}(cydta)(H_2O)]^{2-}$ and pK_a Values for the Acid Dissociation of $[Fe^{II}(Hcydta)(H_2O)]^-$ with Reference Values from the Literature

$\log \beta^{III}_{110}$	$\log \beta^{II}_{110}$	pK^{II}_{a1H}	ref
29.05 ± 0.01	17.96 ± 0.01	2.69	this work[a]
29.27	18.20		34[b]
28.05			35[c]
29.77			36[d]
		2.88	37[e]

[a] 25 °C, 0.1 M KNO_3. [b] 25 °C, 0.1 M KCl. [c] 20 °C, 0.1 M $NaClO_4$. [d] 25 °C, 0.1 M $NaClO_4$. [e] 25 °C, 1.0 M $NaClO_4$.

value for the complex formation of Fe^{III}edta with the value reported by Doi.[40] Doi tried to verify the correctness of his value by a comparison of his $\Delta S°$ for Fe^{III}edta with that of Al^{III}edta.[48,49] This comparison cannot be considered reasonable because there is a large difference between the ionic radii of Al^{III} (0.535 Å) and Fe^{III} (0.645 Å),[50] leading to the expected higher $\Delta S°$ values for the formation of aluminum(III) complexes as compared to those of iron(III) complexes.

We consider our data for Fe^{III}edta to be more reliable based on the following arguments. The increase in $\Delta S°$ on going from M^{II}edta to M^{II}cydta complex formation for divalent 3d M^{II} Irving–Williams ions from Mn^{II} to Zn^{II} can be expressed by the mean value $\Delta(\Delta S°_{cydta-edta})_{av} = 80 \pm 11$ J K^{-1} mol^{-1},[48,51,52] showing that the $\Delta S°$ term for cydta complex formation is always significantly more positive than that of edta because cydta is more preorganized for complex formation and loses much less translation entropy than edta (cf., e.g., Chart I in ref 53). Our $\Delta(\Delta S°_{cydta-edta}) = 106$ J K^{-1} mol^{-1} and is thus more realistic than the difference found by Doi.[40] In addition, for a particular metal ion, the formation enthalpies for edta complexes are usually more exothermic than those of their cydta counterparts,[48,51,52] in agreement with the trend of our data for edta and cydta.

2.2. Determination of pK_{a1OH} and the Dimerization Constant K_d for $[Fe^{III}(cydta)(H_2O)]^-$ from pH-Dependent Spectrophotometric Titrations. Equilibrium constants of this type are traditionally estimated by means of pH potentiometric titrations where variation of the total complex concentration enables the exact evaluation of K_d.[38] In the present work, a new approach for the simultaneous evaluation of pK^{III}_{a1OH} [reaction (5)] and K_d/K_D [reactions (6a) and (6b)] was applied that makes use of the pH and complex concentration dependencies of the very intense absorption bands in the near-UV (borderline between UV and visible ranges). These bands, which are typical for $Fe-O_\mu-Fe$ dimers, were initially assigned as "simultaneous pair excitations" of single, spin-forbidden, ligand-field states that should become spin-allowed by interactions via the oxo bridge.[54,55] Later it was demonstrated that these bands belong to $O_{oxo} \rightarrow Fe^{3+}$ charge-transfer (CT) bands of $Fe-O_\mu-Fe$ dimers.[56,57]

The hydrolysis of Fe^{III}cydta under weakly alkaline conditions is peculiar compared to that of Fe^{III}edta and

(49) Moeller, T.; Chu, S.-K. *J. Inorg. Nucl. Chem.* **1966**, *28*, 153–159.
(50) Shannon, R. D. *Acta Crystallogr., Sect. A: Found. Crystallogr.* **1976**, *A32*, 751–767.
(51) Anderegg, G. *Helv. Chim. Acta* **1963**, *46*, 2813–2822.
(52) Wright, D. L.; Holloway, J. H.; Reilley, C. N. *Anal. Chem.* **1965**, *37*, 884–892.
(53) Evers, A.; Hancock, R. D.; Martell, A. E.; Motekaitis, R. J. *Inorg. Chem.* **1989**, *28*, 2189–2195.
(54) Schugar, H. J.; Rossman, G. R.; Barraclough, C. G.; Gray, H. B. *J. Am. Chem. Soc.* **1972**, *94*, 2683–2690.
(55) Schugar, H. J.; Rossman, G. R.; Thibeault, J.; Gray, H. B. *Chem. Phys. Lett.* **1970**, *6*, 26–28.
(56) Reem, R. C.; McCormick, J. M.; Richardson, D. E.; Devlin, F. J.; Stephens, P. J.; Musselman, R. L.; Solomon, E. I. *J. Am. Chem. Soc.* **1989**, *111*, 4688–4704.
(57) Brown, C. A.; Remar, G. J.; Musselman, R. L.; Solomon, E. I. *Inorg. Chem.* **1995**, *34*, 688–717.

Table 4. Comparison of the Thermodynamic Data for the Complex Formation of Fe^{III}cydta Determined in This Work with Values for Fe^{III}edta (25 °C, I = 0.1 M KNO_3)

	$\log \beta_{110}$	$\Delta G°$ [kJ mol^{-1}]	$\Delta H°$ [kJ mol^{-1}]	$\Delta S°$ [J K^{-1} mol^{-1}]	source
$[Fe(cydta)(H_2O)]^-$	29.05 ± 0.01	−165.8	−23 ± 1	480	this work[b]
	29.77	−169.9	−25.1	486	36[a]
$[Fe(edta)(H_2O)]^-$	24.95 ± 0.01	−142.4	−31 ± 1	374	41[b]
	25.00	−142.7	−11.5 ± 0.5	440	40[a]

[a] 25 °C, I = 0.1 M $NaClO_4$. [b] 25 °C, I = 0.1 M KNO_3.

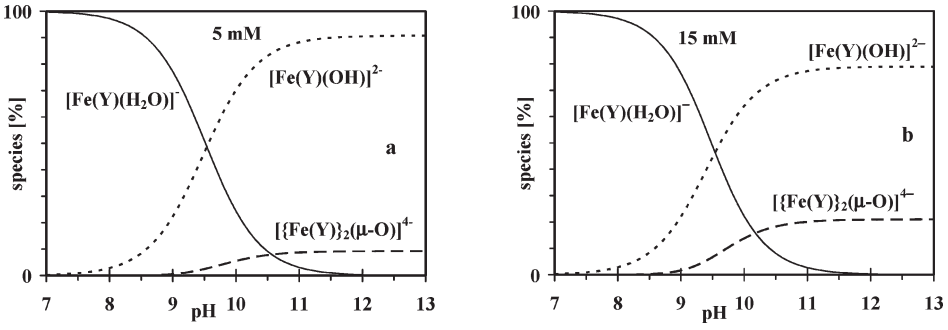

Figure 5. pH-dependent speciation of Fe^{III}cydta as a function of the pH 7−13 and the total complex concentration $[Fe(cydta)]_T$: (a) 5 mM; (b) 15 mM. Computations based on pK^{III}_{a1OH} = 9.54 and pK_D = 18.03 (log K_d = 1.07).

related complexes[58,59] because deprotonation of the metal-coordinated water takes place at pH values two units higher than in the case of Fe^{III}edta and the dimerization constant K_d [cf. reaction (6b)] is also two log units lower than that in the latter case.[38,39] Especially, the small dimerization tendency required a special approach; viz., higher complex concentrations than in the case of the Fe^{III}edta dimer titrations are required to visualize the dimer bands.[41] This is necessary to attain appropriate precision during spectral evaluation of the pH-dependent spectra with SPECFIT (further details illustrating this point are presented in the Supporting Information).

$$[Fe^{III}(cydta)(H_2O)]^- \overset{K^{III}_{a1OH}}{\rightleftharpoons} [Fe^{III}(cydta)(OH)]^{2-} + H^+ \quad (5)$$

$$2[Fe^{III}(cydta)(H_2O)]^- \overset{K_D}{\rightleftharpoons} [\{Fe^{III}(cydta)\}_2(\mu\text{-}O)]^{4-} + H_2O + H^+ \quad (6a)$$

$$2[Fe^{III}(cydta)(OH)]^{2-} \overset{K_d}{\rightleftharpoons} [\{Fe^{III}(cydta)\}_2(\mu\text{-}O)]^{4-} + H_2O \quad (6b)$$

An interesting observation made during pH-dependent spectrophotometric titrations (see Figure S5 in the Supporting Information) concerns the isosbestic point at 310 nm. This feature was not observed during the study of the analogous Fe^{III}edta system.[8] The reason for this difference can be explained with the details shown in Figures 5a,b, where the species distribution of Fe^{III}cydta for the conditions of Figure S4 in the Supporting Information are depicted. These species distributions reveal that dimer formation starts in both cases only at pH > 9. At a lower total complex concentration of 5 mM, the concentration profiles reach a limiting value in both cases at pH ∼ 11, where 9.2 and 20.9% of the total Fe^{III}cydta are present as dimer, respectively.

Figure 6a presents the limiting spectra computed with SPECFIT[60−63] for the three protolytic species $[Fe(cydta)(H_2O)]^-$, $[Fe(cydta)(OH)]^{2-}$, and $[\{Fe(cydta)\}_2(\mu\text{-}O)]^{4-}$, whereas the pH dependence of the molar absorbance at 285 nm is shown in Figure 6b for both series. From the spectrum of $[\{Fe(cydta)\}_2(\mu\text{-}O)]^{4-}$ in Figure 6a, the three typical CT bands are visible as spectroscopic signatures for the presence of a μ-oxo-bridged dimer.[56,57] A comparison of our data estimated for the equilibrium constants of reactions (4) and (5) with data from the literature is made in Table 5. This compilation reveals a reasonable agreement, especially between our values for pK^{III}_{a1OH} and log K_d and those published by Gustafson and Martell.[38]

An understanding of the differences in protolytic properties between Fe^{III}cydta and Fe^{III}edta can be attained if the protolytic properties of Fe^{III}pdta (where pdta = 1,2-propanediaminetetraacetate) are included in the appropriate compilation. A comparison of these data is shown in Table 6.[41]

Especially important for a proper understanding of the structural changes that accompany the Fe^{III}cydta hydrolytic reactions is the dependence of pK^{III}_{a1OH} on the ligand architecture. For a better understanding of the structural differences between these chelates, the appropriate ligands and structures of the starting complexes in these protolytic systems are summarized in Scheme 1.

(58) Schugar, H. J.; Walling, C.; Jones, R. B.; Gray, H. B. *J. Am. Chem. Soc.* **1967**, *89*, 3712–3720.
(59) Schugar, H. J.; Hubbard, A. T.; Anson, F. C.; Gray, H. B. *J. Am. Chem. Soc.* **1969**, *91*, 71–77.
(60) Gampp, H.; Maeder, M.; Meyer, C. J.; Zuberbuehler, A. D. *Talanta* **1985**, *32*, 1133–1139.
(61) Gampp, H.; Maeder, M.; Meyer, C. J.; Zuberbuehler, A. D. *Talanta* **1985**, *32*, 95–101.
(62) Gampp, H.; Maeder, M.; Meyer, C. J.; Zuberbuehler, A. D. *Talanta* **1986**, *33*, 943–951.
(63) Gampp, H.; Maeder, M.; Meyer, C. J.; Zuberbuhler, A. D. *Talanta* **1985**, *32*, 251–264.

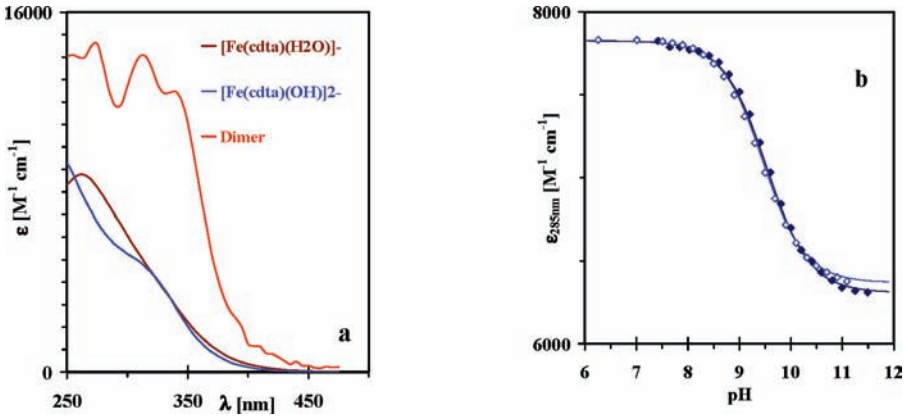

Figure 6. (a) Limiting spectra computed with SPECFIT[60−63] for $[Fe(cydta)(H_2O)]^-$, $[Fe(cydta)(OH)]^{2-}$, and $[\{Fe(cydta)\}_2(\mu\text{-}O)]^{4-}$ based on the data shown in Figure 5. (b) pH dependence of $\varepsilon_{285\ nm}$ (molar extinction at 285 nm): (◆) $[Fe(cydta)]_T = 5$ mM; (◇) $[Fe(cydta)]_T = 15$ mM. Lines shown result from the data fits.

Table 5. Equilibrium Constants for the Formation of $[Fe(cydta)(OH)]^{2-}$ and $[\{Fe(cydta)\}_2(\mu\text{-}O)]^{4-}$ Estimated from pH-Dependent Spectrophotometric Titrations and SPECFIT[60−63] Evaluation Compared with Reference Data from the Literature

source	this work [a] (25 °C, 1.0 M KNO_3)	ref 38[b] (25 °C, 1.0 M KCl)	ref 39[c] (25 °C, 1.0 M $NaNO_3$)	ref 35[d] (20 °C, 0.1 M $NaClO_4$)
pK^{III}_{a1OH}	9.54 ± 0.01	9.32	≈9	9.70
$\log K_d$	1.07	1.01	1.00	
$-\log K_D$	18.03 ± 0.06	17.62	17.00	

[a] Spectrophotometric titration (SPECFIT). [b] pH-potentiometric titration. [c] Kinetic measurements. [d] Redox measurements.

Table 6. Comparison of the pK_{a1OH} and K_d Values for Fe^{III}cydta with those of Fe^{III}edta and Fe^{III}pdta

	Fe^{III}edta	Fe^{III}pdta	Fe^{III}cydta
pK^{III}_{a1OH}	7.52 ± 0.01	7.70 ± 0.01	9.54 ± 0.01
$\log K_d$	2.64	2.28	1.07
$-\log K_D$	12.40 ± 0.05	13.12 ± 0.06	18.03 ± 0.06

The features that become apparent from the different shapes of the pK^{III}_{a1OH} dependence on the ligand architecture of the three iron(III) complexes are best explained on the basis of the details shown in Scheme 2.

The model shown in Scheme 2 is similar to an earlier model that was used to explain the hydroxo complex formation of the related *u-fac*-$[Fe(ida)_2]^-$ complex as the starting species. In that model, the existence of seven-coordinate $[Fe(ida)_2(H_2O)]^-$ with an iron-bound water in the starting solutions was assumed to account for hydroxo complex formation at near-neutral pH.[64] The overall reaction (7) comprises an aquation reaction on the left-handed side, which initiates an autoprotolytic process on the product site. The water molecule initially attacks the six-coordinate complex $[Fe^{III}(cydta)]^-$ to form $[Fe^{III}(cydta)(H_2O)]^-$, which is deprotonated in the course of the reaction. The ternary hydroxo complex thus formed can formally exist either as a seven-coordinate species or as a six-coordinate, ring-opened hydroxo complex. The apparent equilibrium between these two species cannot be presented by the formula $[Fe^{III}(cydta)(OH)]^{2-}$ (cf. structures of ring-opened and ring-closed species of $[Fe^{III}(OH)]^{2-}$ in Scheme 2).

$$[Fe^{III}(cydta)]^- + H_2O \overset{K^{III}_{a1OH}}{\rightleftharpoons} [Fe^{III}(cydta)(OH)]^{2-} + H^+ \quad (7)$$

Our model does not contain a chelate ring-opened species on the side of the mononegatively charged starting species of reaction (7) because ring opening of a metal complex glycinate chelate ring in an aqueous solution is connected to an unfavorable entropy change because the negative charge on the carboxylate group attracts numerous water molecules through electrostriction.[65,66]

The only process that has to be considered at pH < 8 for the case in which the commonly valid Scheme 2 is applied to Fe^{III}cydta is the water-exchange reaction (8), which corresponds to the horizontal transition on the left-hand side in Scheme 2. Details concerning reaction (8) for Fe^{III}cydta and Fe^{III}edta are discussed in the next section, which reports the details of the water-exchange kinetics studied with temperature- and pressure-dependent ^{17}O NMR spectroscopy. The only feature that we need to consider at this point is the fact that equilibrium (8) lies far on the right-hand side for both Fe^{III}edta and Fe^{III}cydta.

$$[Fe^{III}(cydta)]^- + H_2O \overset{K_{6\rightarrow7}}{\rightleftharpoons} [Fe^{III}(cydta)(H_2O)]^- \quad (8)$$

The active species that is deprotonated is the seven-coordinate complex $[Fe^{III}(cydta)(H_2O)]^-$, yielding a seven-coordinate hydroxo complex $[Fe^{III}(cydta)(OH)]^{2-}$ along the horizontal acid−base equilibrium in the upper part of Scheme 2, to which the microequilibrium constant $K_{a7/7}$ [reaction (9)] has been assigned.

$$[Fe^{III}(cydta)(H_2O)]^- \overset{K_{a7/7}}{\rightleftharpoons} [\{Fe^{III}(cydta)(OH)\}_{CN7}]^{2-} + H^+ \quad (9)$$

(64) Powell, A. K.; Heath, S. L. *Comments Inorg. Chem.* **1994**, *15*, 255–296.

(65) van Eldik, R. *Coord. Chem. Rev.* **1999**, *182*, 373–410.

(66) (a) Yoshitani, K. *Bull. Chem. Soc. Jpn.* **1994**, *67*, 2115–2120. (b) Beswick, C. L.; Shalders, R. D.; Swaddle, T. W. *Inorg. Chem.* **1996**, *35*, 991–994.

Scheme 1. Comparison of the Ligands edta, pdta, and cydta and the Structures Resulting from Monomeric Complexes with Fe^{III}

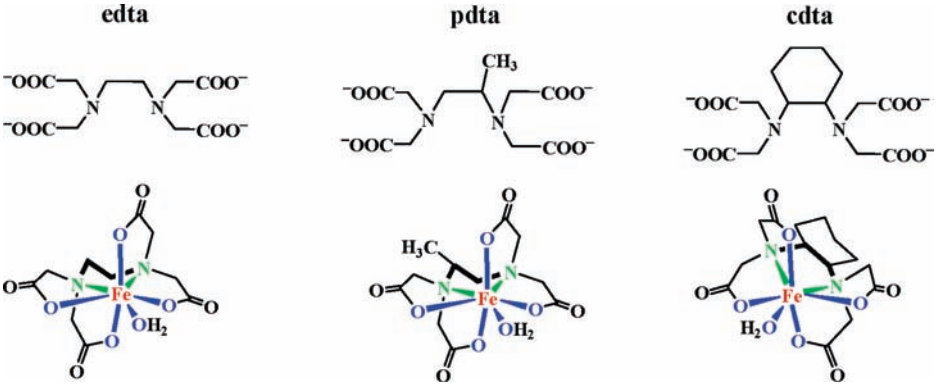

Scheme 2. Common Model for Equilibrium and Structural Changes during the Formation of Ternary Metal−edta−Hydroxo Complexes

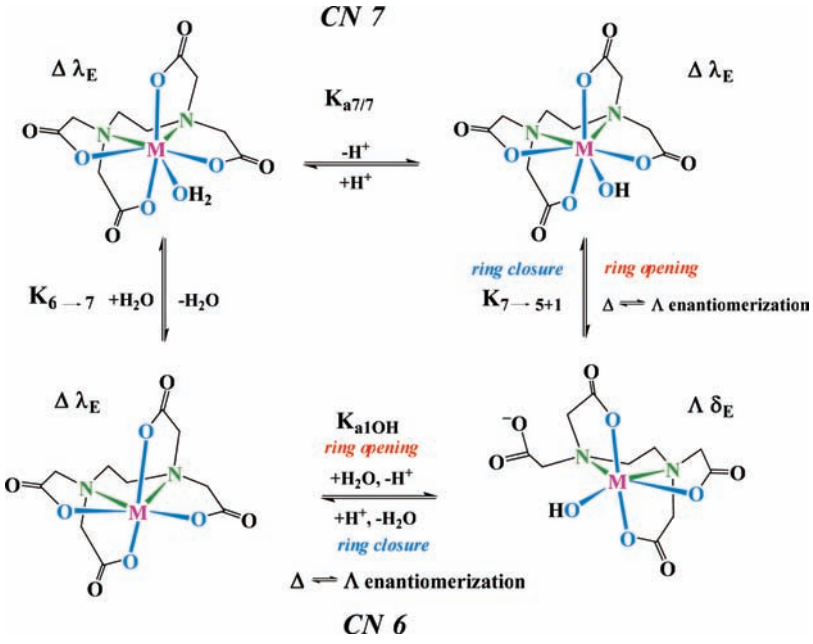

$$[\{Fe^{III}(cydta)(OH)\}_{CN\,7}]^{2-} \overset{K_{7\rightarrow 5+1}}{\rightleftharpoons} [\{Fe^{III}(cydta)(OH)\}_{CN\,5+1}]^{2-} \quad (10)$$

The short Fe−OH bond in the product species of reaction (9) and the need for the presence of three orbitals with π symmetry at the metal site in the ternary hydroxo complexes (only two such orbitals are encountered in the seven-coordinate complexes)[67] are thought to be responsible for the fact that the vertical right-hand path in Scheme 2 is favored to proceed from the upper part to the lower part [or from the left to the right in reaction (9)] if $K_{7\rightarrow 5+1} \gg 1$, the equilibrium constant of reaction (10). Reaction (10) is thought to take place with complete enantiomerization of the protolytically active species, and the chiralities of all chelate rings undergo $\delta \rightleftharpoons \lambda$ switches. These ideas are based on some archetypical observations:

(i) The opening of a single glycinate chelate ring by a six-coordinate edta complex (e.g., $[Co^{III}(edta)]^-$) accompanied by anation of a ternary ligand X^- and formation of $[Co^{III}(edta)X]^{2-}$ does not lead to enantiomerization, but retention is observed instead.[68,69]

(ii) If the pH is increased, however, in the protolytic system of $[Co^{III}(edta)]^-$, acceleration of enantiomerization is observed and the rate of the reaction becomes dependent upon the OH^- concentration. The overall process was classified as an associative, OH^--catalyzed racemization.[69]

If these features are adapted to the situation in Scheme 2, it is clear that ring opening can take place only at the CN 7 level and optimal reaction conditions are met if the ligand coordinated to the protolytic species does not exert any counteraction to the chelate ring flips. If this were the case, the enantiomerization and, in turn, the chelate ring-opening process would be hindered, leading to a much smaller value of $K_{7\rightarrow 5+1}$ and an increase in the overall pK_{aIOH} [cf. reaction (11)]. This feature is

(67) Hoffmann, R.; Beier, B. F.; Muetterties, E. L.; Rossi, A. R. *Inorg. Chem.* **1977**, *16*, 511–522.

(68) Busch, D. H.; Cooke, D. W. *J. Inorg. Nucl. Chem.* **1961**, *23*, 145–148.

(69) Cooke, D. W.; Im, Y. A.; Busch, D. H. *Inorg. Chem.* **1962**, *1*, 13–15.

thought to be responsible for the large difference between the pK_{a1OH} values of $[Fe^{III}(edta)(H_2O)]^-$ and $[Fe^{III}(cydta)(H_2O)]^-$, whose coordinated water molecules should have approximately the same Brönsted acidity strength (cf. the discussion of the structural features of the salts of the complex anions in the previous section and further points described below). Specific coupling of the three equilibria can lead to peculiar pK_{a1OH} values for any system that can be quantified experimentally. This is especially true if $K_{6\rightarrow7}$ and $K_{7\rightarrow5+1}$ show extreme values because in these cases the nature of the expected simple acid−base reaction is lost in favor of a cascade of reactions controlled by the water exchange and CN changes realized by ring-opening reactions.

$$K_{a1OH} = K_{6\rightarrow7} \cdot K_{a7/7} \cdot K_{7\rightarrow5+1} \qquad (11)$$

In summary, it can be stated that the pK^{III}_{a1OH} value that can be measured experimentally is an overall equilibrium constant, as expressed in eq 11, consisting of the three consecutive preceding reactions (8)−(10). If in such a protolytic system with L = edta, pdta, and cydta, $K_{6\rightarrow7}$ is large in all three cases and the $K_{a7,7}$ values are of similar magnitude (as is the case for the three Fe^{III}−Y systems), as we assumed, and also all $K_{7\rightarrow5+1}$ values are extremely small, only seven-coordinate types of $[Fe^{III}(L)(OH)]^{2-}$ species will be present in solution. This means that equilibrium (9) is far on the side of the products while equilibrium (10) is far on the side of the reactants.

Such behavior is obviously shown by a number of seven-coordinate iron(III) complexes with ligands from subfamilies of *o*-phenylendiaminetetraacetate (*o*-phdta). In these systems, no μ-oxo dimers could be detected.[70] This is a tantalizing hint that the active species in the course of dimer formation is always the six-coordinate ring-opened hydroxo species $[\{M^{III}(L)(OH)\}_{5+1}]^{2-}$.[41] In turn, such protolytic systems would be described sufficiently by only the upper path of Scheme 2 [reaction (9)] provided that the equilibrium constant $K_{6\rightarrow7}$ is large enough.

For the three Fe^{III}−L systems with L = edta, pdta, and cydta, a slight increase in pK^{III}_{a1OH} is noted on going from Fe^{III}edta to Fe^{III}pdta. This change is related to the extra methyl group in the ligand backbone and could hinder the $\delta \rightleftharpoons \lambda$ interconversion of the central diamine chelate ring by changing the CH_3 orientations from the energetically favorable equatorial position to the unstable axial position. An increase by 2 log units in the pK_{a1OH} is noted on going from Fe^{III}edta to Fe^{III}cydta. Now, the path belonging to reaction (10) is almost completely blocked because the opportunity of central diamine chelation to occur a $\delta \rightleftharpoons \lambda$ flip is completely frozen. The increase in pK_{a1OH} is, as we believe, almost completely driven by a now much smaller value for $K_{7\rightarrow5+1}$ as compared to the Fe^{III}edta system. This leads to a much larger equilibrium fraction of the seven-coordinate hydroxo complex of $[Fe^{III}(cydta)(OH)]^{2-}$ as compared to that of the edta system, and the amount of the related six-coordinate, ring-opened hydroxo species is drastically diminished. These counterbalanced changes are responsible for the drop in log K_d from 2.64 for Fe^{III}edta to 1.07 in the case of Fe^{III}cydta. This argumentation in terms of the three $Fe^{III}(Y)$ protolytic systems and the differing nature of $[Fe^{III}(Y)(OH)]^{2-}$ equilibrium mixtures (i.e., composed of fractions of seven-coordinate and ring-opened six-coordinate hydroxo complexes) is further supported by inspection of Figure 7, which shows the limiting spectra for the $[Fe^{III}(Y)(OH)]^{2-}$ protolytic species as computed by SPECFIT.[41]

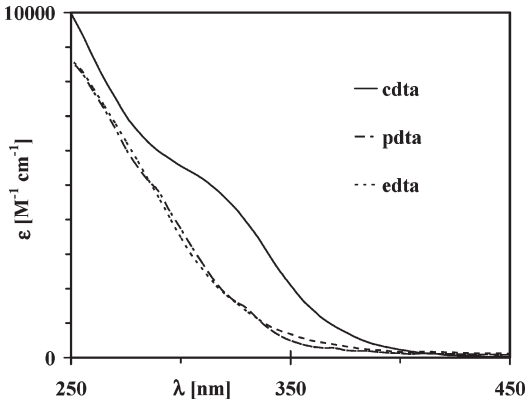

Figure 7. Comparison of the limiting spectra of the protolytic species $[Fe(cydta)(OH)]^{2-}$, $[Fe(pdta)(OH)]^{2-}$, and $[Fe(edta)(OH)]^{2-}$ as computed by SPECFIT. Each spectrum is, according to the model in Scheme 2, a composite spectrum of the pair of seven-coordinate and ring-opened six-coordinate hydroxo complexes.

Table 7. Activation Parameters Resulting from the Least-Squares Fit of $1/T_{2r}$ as a Function of the Temperature for $[Fe^{III}(cydta)(H_2O)]^-$ and $[Fe^{III}(edta)(H_2O)]^-$ at pH 5.0

	$[Fe^{III}(cydta)(H_2O)]^-$	$[Fe^{III}(edta)(H_2O)]^-$
$\Delta H^{\ddagger}$ [kJ mol^{-1}]	40.2 ± 1.3	24.0 ± 0.2
$\Delta S^{\ddagger}$ [J mol^{-1} K^{-1}]	+28 ± 5	−15.4 ± 0.7
$\Delta G^{\ddagger}$ at 298 K [kJ mol^{-1}]	31.7	28.6
k_{ex} at 298 K [s^{-1}]	(1.7 ± 0.2) × 10^7	(6.0 ± 0.1) × 10^7
$\Delta V^{\ddagger}$ [cm^3 mol^{-1}]	+2.3 ± 0.1	+3.6 ± 0.1

3. Details of the Water-Exchange Mechanism of $[Fe^{III}(cydta)(H_2O)]^-$ as Compared to $[Fe^{III}(edta)(H_2O)]^-$. The water-exchange kinetics of $[Fe^{III}(edta)(H_2O)]^-$ and $[Fe^{III}(cydta)(H_2O)]^-$ were studied by our group before.[71] We have now extended these measurements by applying the variable-temperature/variable-pressure ^{17}O NMR technique under different conditions, viz., pH 5.0 in the present work as compared to pH 4.0 in the earlier work. Furthermore, the former experiments were solely based on the use of the line-broadening technique to evaluate the appropriate rate data. To reach a higher precision, we now included the shift of the ^{17}O NMR resonance as a function of the temperature and pressure in the measurement procedure. This approach is of special importance if line-broadening data are not precise enough for an accurate data-fitting procedure. Our shift analysis shows a good agreement with the line-broadening experiments. Inflection points in the plots for $\Delta\omega_r$ occur at the same temperatures where maxima can be seen in the line-broadening plots. This confirms clearly a changeover from the slow to the fast exchange region. The parameters

(70) Sanchiz, J.; Dominguez, S.; Mederos, A.; Brito, F.; Arrieta, J. M. *Inorg. Chem.* **1997**, *36*, 4108–4114.

(71) Schneppensieper, T.; Seibig, S.; Zahl, A.; Tregloan, P.; van Eldik, R. *Inorg. Chem.* **2001**, *40*, 3670–3676.

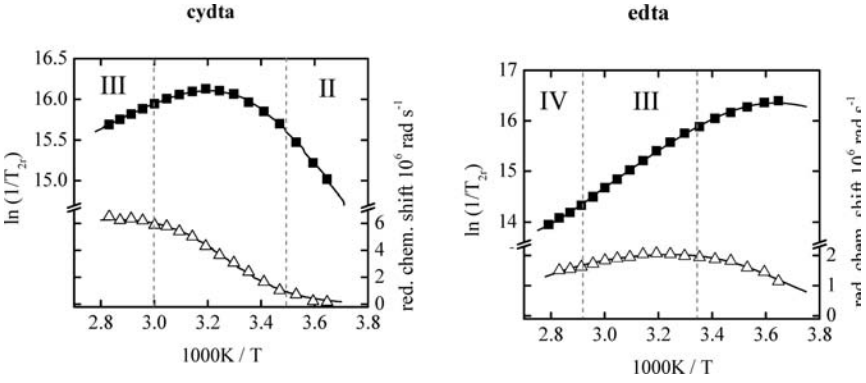

Figure 8. Temperature dependence of the reduced transverse relaxation rate (■) and the reduced chemical shift difference $\Delta\omega_r$ (△) of the ^{17}O NMR resonances for $[Fe^{III}(cydta)(H_2O)]^-$ (top) and $[Fe^{III}(edta)(H_2O)]^-$ (bottom). The solid lines result from simultaneous nonlinear fits of line-broadening and shift experiments with the Swift−Connick equation (for further details, see the Supporting Information).

Scheme 3. Differences between the Water-Exchange Reactions of $[Fe^{III}(cydta)(H_2O)]^-$ (top, the Ligand Acting here is (*S*,*S*)-cydta) and $[Fe^{III}(edta)(H_2O)]^-$ (bottom)

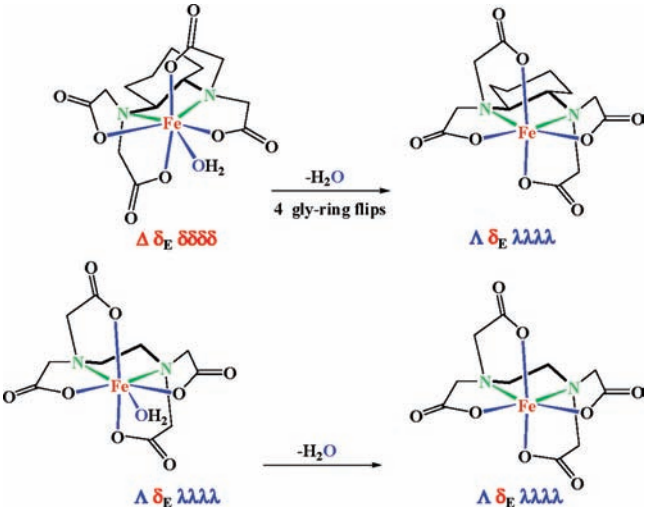

obtained from the fitting routine for the line-broadening data were used to calculate the temperature dependence of the reduced shift $\Delta\omega_r$. A comparison of calculated and measured data shows good agreement between these independent experiments. The parameters obtained in the present study (see Table 7) are close to those reported in the foregoing study,[71] where only the line-broadening approach had been applied. Details of the various kinetic measurements are collected in Figure 8.

It is apparent from the data in Table 7 that the mechanism for the water-exchange reaction for $[Fe^{III}(cydta)(H_2O)]^-$ are similar to those for $[Fe^{III}(edta)(H_2O)]^-$. In both cases, the character of the exchange process is of the I_d (interchange dissociative) type because the activation volumes $\Delta V^{\ddagger}$ have small but significantly positive values in both cases. The water-exchange rate is about 3 times[72] faster for the edta complex. This difference can be rationalized on the basis of the structural peculiarities of the cydta versus edta ligand. As shown in Scheme 3, water exchange in the case of $[Fe^{III}(edta)(H_2O)]^-$ only involves cleavage of the $Fe^{III}-OH_2$ bond. This differs from the situation in $[Fe^{III}(cydta)(H_2O)]^-$. As mentioned above, any change in the coordination number from 6 to 7 or vice versa in a (*R*,*R*)- or (*S*,*S*)-cydta complex requires the concomitant flip of the four glycinate rings in the hexadentate coordinating cydta ligand.

The appropriate ring flips seem to consume less energy than we initially suspected because this sort of dynamics has been observed in ^1H NMR studies on the cydta complexes of Sc^{III}, Mg^{II}, In^{III}, and Pb^{II} in aqueous solution.[73] In the latter, the rate of acetate scrambling illustrated in the upper part of Scheme 3 on going from the seven- to six-coordinate cydta complex is drastically increased in solutions of Sc^{III}cydta if the temperature is increased from room temperature to values near the boiling point of water.

4. Mössbauer Spectral Studies of Reactants and Products of the Protolytic Reactions of Fe^{III}cydta and Its Ternary Peroxo Complexes. Additional details and background information for the performed studies are given in the Supporting Information. The frozen solution Mössbauer spectra of the Fe^{III}cydta system at pH 8.1 and 10.4 without H_2O_2 added are shown in Figure 9. At pH 8.1, the dominance of the $[Fe^{III}(cydta)(H_2O)]^-$ species is expected, whereas at pH 10.4, deprotonation can occur and result in the formation of $[Fe^{III}(cydta)(OH)]^{2-}$. At pH 8.1, the spectrum is a combination of a sextet and a relaxation-distorted subspectrum. The latter was evaluated by the Blume−Tjon model as an approximation, implemented in the Mosswinn code;[74] the parameters are not discussed because of the difficulties mentioned above (further details are presented in the Supporting Information). The sextet is well-resolved, and its high isomer shift (0.57 mm/s, A_1 in Table 8) indicates 7-fold coordination. The connection between the isomer shift and the coordination number in similar systems has been studied by Takeda.[75] Mössbauer features of all species in our experiments are listed in Table 8. It is straightforward to assign this sextet to the $[Fe^{III}(cydta)(H_2O)]^-$ monomer in agreement with the virtually identical data set obtained for its parent solid (A_2 in Table 8). The relaxation subspectrum may be assigned to the same species (to those ions that are statistically closer to each other, and thus the magnetic field starts to collapse), but other

(72) Meier, R.; Kallies, B., unpublished results.

(73) Mirti, P.; Gennaro, M. C. *Spectrosc. Lett.* **1983**, *16*, 741–751.
(74) Klencsar, Z.; Kuzmann, E.; Vertes, A. *J. Radioanal. Nucl. Chem.* **1996**, *210*, 105–118.
(75) Takeda, M. *Hyperfine Interact.* **1986**; *28*, 737−740.

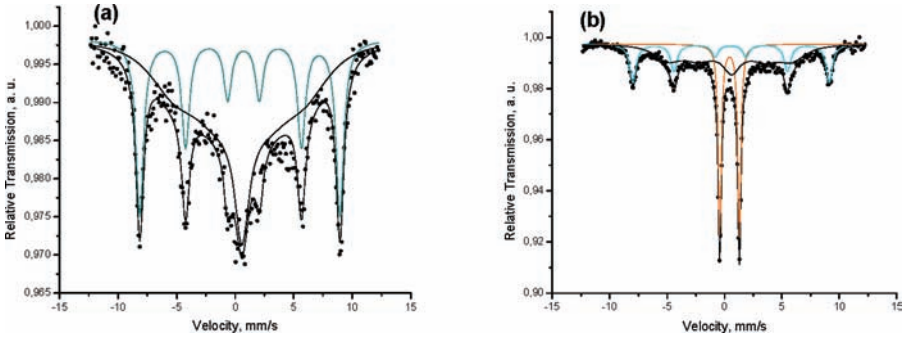

Figure 9. Frozen-solution Mössbauer spectra of the Fe^{III}cydta system at pH 8.1 (a) and 10.4 (b). Experimental conditions: (a) $[Fe(cydta)(H_2O)^-] = 0.021$ M, $T = 83$ K; (b) $[Fe(cydta)(OH)^{2-}] = 0.021$ M, $T = 83$ K.

Table 8. Mössbauer Parameters of the Fe^{III} Species Observed in the Fe^{III}cydta$-H_2O_2$ System at 83(2) K

species observed	Mössbauer parameters			
	δ (mm/s)	Δ (mm/s)	2ε (mm/s)	B (T)
A_1 $[Fe^{III}(cydta)(H_2O)]^-$ monomer	0.57(2)		−0.25	53.0(5)
A_2 $K[Fe^{III}(cydta)(H_2O)]\cdot 3H_2O$ solid-state sample	0.55(2)	0.75(1)		
B $[Fe^{III}(cydta)(OH)]^{2-}$ monomer	0.55(1)		+0.06(2)	52.8(5)
C $[\{Fe^{III}(cydta)\}_2(\mu\text{-}O)]^{4-}$ dimer	0.44(1)	1.69(1)		0
D $[Fe^{III}(cydta)(\eta^2\text{-}O_2)]^{3-}$ monomer	0.61(2)	0.80(1)		50.2(5)
E $[\{Fe^{III}(cydta)\}_2(\mu\text{-}O_2)]^{4-}$ peroxo-bridged species	0.48	0.79		0

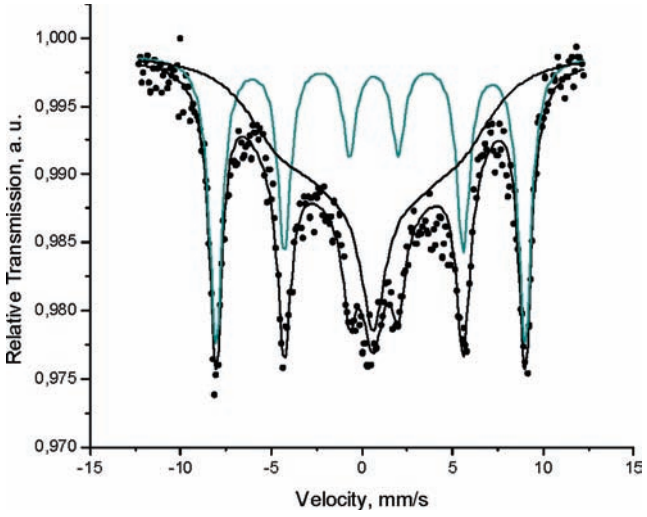

Figure 10. Frozen-solution Mössbauer spectrum of the Fe^{III}cydta system at pH 8.4 after the addition of H_2O_2 without the formation of $[Fe^{III}(cydta)(\eta^2\text{-}O_2)]^{4-}$. Experimental conditions: $[Fe(cydta)(H_2O)^-] = 0.021$ M, pH 8.4, excess H_2O_2, $T = 83$ K.

minor species showing up only in relaxation cannot be excluded.

At pH 10.4, the spectrum is very different; in addition to a relaxation component, a sextet and a doublet are now observed. The isomer shift and the hyperfine magnetic field of the sextet are the same as those observed for $[Fe^{III}(cydta)(H_2O)]^-$, but the quadrupole shift (2ε) is markedly different (see Table 8). This difference is consistent with the assumption that this species is really the deprotonated form of $[Fe^{III}(cydta)(H_2O)]^-$, viz., $[Fe^{III}(cydta)(OH)]^{2-}$ (B in Table 8). The fact that only the quadrupole interaction differs upon deprotonation shows that protonation/deprotonation does not alter the 3d density on the Fe^{3+} center appreciably but the electric charge of the OH^- ion causes a slight distortion of the ligand sphere. This is another hint that the species $[Fe^{III}(cydta)(OH)]^{2-}$ is predominantly seven-coordinate in solution with equilibrium (10) (cf. above) shifted appreciably to the right.

The sharp doublet with parameters $\delta = 0.44$ mm/s and $\Delta = 1.69$ mm/s (C in Table 8) almost perfectly matches the parameters of the $[\{Fe(edta)\}_2(\mu\text{-}O)]^{4-}$ dimeric species; the quadrupole splitting is higher by about 0.09 mm/s. The isomer shift obviously indicates 6-fold coordination; thus, one carboxylate arm of the cydta chelate must be detached from the iron center on each side of the dimer analogously to the Fe(edta) complex.

In an attempt to produce $[Fe^{III}(cydta)(\eta^2\text{-}O_2)]^{3-}$, H_2O_2 was added to the Fe^{III}cydta system at pH 8.4. The color of the solution changed only within the shades of yellow, and the Mössbauer spectrum recorded (Figure 10) was an almost perfect reproduction of that of the sample at pH 8.1 without the addition of H_2O_2. The parameters of the well-resolved sextet ($\delta = 0.56$ mm/s, $2\varepsilon = -0.19$ mm/s, and $B = 52.9$ T) confirmed the presence of $[Fe^{III}(cydta)H_2O]^-$.

At pH 11.6, the addition of H_2O_2 resulted in an intense purple coloration that immediately started to fade, but the sample could be quenched to liquid-nitrogen temperature before it turned yellow. The spectrum obtained is reported in Figure 11a. In a second trial, the system was cooled in an ice bath before the addition of H_2O_2. The coloration was more intense and more stable, and the resulting Mössbauer spectrum is presented in Figure 11b. The latter spectrum is strikingly similar to the one obtained in the analogous experiment with edta.[11] The isomer shift of this sextet (D in Table 8) is the highest of all species found ($\delta = 0.61$ mm/s), and the quadrupole shift is very characteristically high positive ($\Delta = +0.8$ mm/s). This sextet can be logically assigned to the seven-coordinate $[Fe^{III}(cydta)(\eta^2\text{-}O_2)]^{3-}$, where cydta is

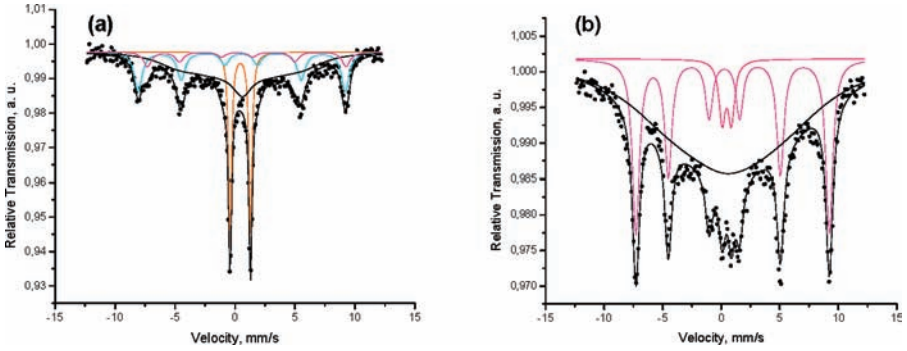

Figure 11. Frozen-solution Mössbauer spectra of the Fe^{III}cydta system at pH 11.4−11.6 after the addition of H_2O_2. Experimental conditions: (a) $[Fe(cydta)(H_2O)^-] = 0.021$ M, pH 11.4, excess H_2O_2, $T = 83$ K; (b) $[Fe(cydta)(OH)^{2-}] = 0.021$ M, pH 11.6, $T = 83$ K.

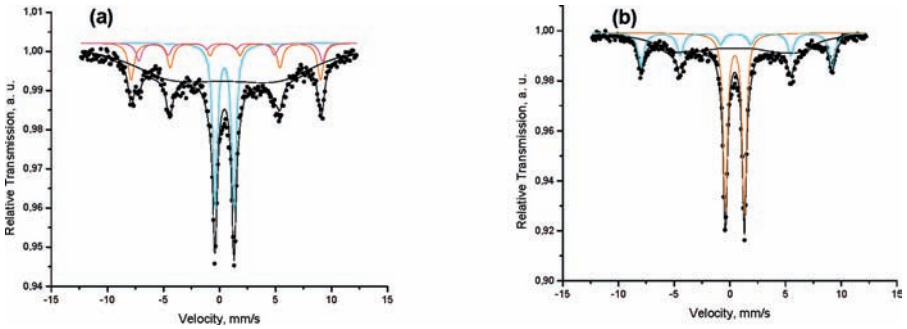

Figure 12. Frozen-solution Mössbauer spectra of the degradation product of the Fe^{III}cydta system at pH 11.4−11.6 after the addition of H_2O_2. Experimental conditions: (a) $[Fe(cydta)(H_2O)^-] = 0.021$ M, pH 11.4, excess H_2O_2, $T = 83$ K; (b) $[Fe(cydta)(OH)^{2-}] = 0.021$ M, pH 11.6, $T = 83$ K.

pentadentate with one carboxylate arm detached and O_2^{2-} is bound side-on. The doublet with parameters $\delta = 0.48$ mm/s and $\Delta = 0.79$ mm/s (E in Table 8) can be tentatively assigned to a peroxo-bridged species, $[\{Fe(cydta)\}_2(\mu\text{-}O_2)]^{4-}$, just as in the case of the edta system, although it should be mentioned that, in contrast to the edta experiments, this species was not observed as a major component in any other spectra.[11]

The spectrum in Figure 11a shows only a relatively weak relaxation background with two sextets and one doublet. The two sextets could be assigned to $[Fe^{III}(cydta)(\eta^2\text{-}O_2)]^{3-}$ and $[Fe^{III}(cydta)OH]^{2-}$, in agreement with the observed faint purple color when the sample was quenched, while the doublet represents the dimer $[\{Fe(edta)\}_2(\mu\text{-}O)]^{4-}$.

The spectra shown in Figure 12 were recorded on the same sample for which the Mössbauer spectrum in Figure 11b is shown, with the difference that for the spectrum in Figure 12a rapid freezing was carried out 3 min after the addition of H_2O_2, whereas for the spectrum in Figure 12b the sample was quenched after an additional several minutes, when the yellow color of the solution completely returned. The pH of this solution was remeasured and found to be 10.4, one unit lower than that before the addition of H_2O_2.

In spectrum (a), the simultaneous presence of $[Fe^{III}(cydta)(\eta^2\text{-}O_2)]^{3-}$, $[Fe^{III}(cydta)OH]^{2-}$, and $[\{Fe(cydta)\}_2(\mu\text{-}O)]^{4-}$ is revealed, whereas in spectrum (b), the sextet of $[Fe^{III}(cydta)(\eta^2\text{-}O_2)]^{3-}$ is absent. These observations are in agreement with the gradual decomposition of the purple peroxo species. After decomposition of H_2O_2 (or part of it), the system returned to its initial state, with somewhat lower pH, characterized by equilibrium (12).

$$2Fe^{III}(cydta)OH]^{2-} \rightleftharpoons [\{Fe(cydta)\}_2(\mu\text{-}O)]^{4-} + H_2O \quad (12)$$

5. Kinetics of the Interaction of $[Fe^{III}(cydta)(H_2O)]^-$ with Hydrogen Peroxide in Comparison to $[Fe^{III}(edta)(H_2O)]^-$. For basic pH values, the addition of H_2O_2 to buffered solutions of $[Fe^{III}(cydta)(H_2O)]^-$ resulted in the formation of a band with $\lambda_{max} = 545$ nm in the UV/vis spectrum. This band can be assigned to the purple Fe−cydta−peroxo complex, for which the color can be plausibly ascribed to a ligand-to-metal CT band. As in the case of $[Fe^{III}(edta)(H_2O)]^-$,[16] the formation of the peroxo complex can only be observed at pH values higher than the pK_a value of the original $[Fe(L)H_2O]^-$ complex. For $[Fe(cydta)(H_2O)]^-$, no overall reaction is observed below a pH of about 10.

Figure 13 shows the spectral changes observed during the reaction of $[Fe(cydta)(H_2O)]^-$ with H_2O_2 at high pH. Kinetic traces recorded at 360 and 550 nm (see Figure 14) show that the reaction clearly consists of two steps. In contrast to $[Fe^{III}(edta)(H_2O)]^-$, not only did the observed rate constants for the first reaction step turn out to depend on the hydrogen peroxide concentration, but also those for the second step showed a slight hydrogen peroxide concentration dependence at pH 11.0 (see further Discussion). Hydrogen peroxide concentration dependences for $[Fe(edta)(H_2O)]^-$ were measured at pH 9.0 and 10.0. During control measurements performed at pH 11.0, it turned out that at pH values close to the

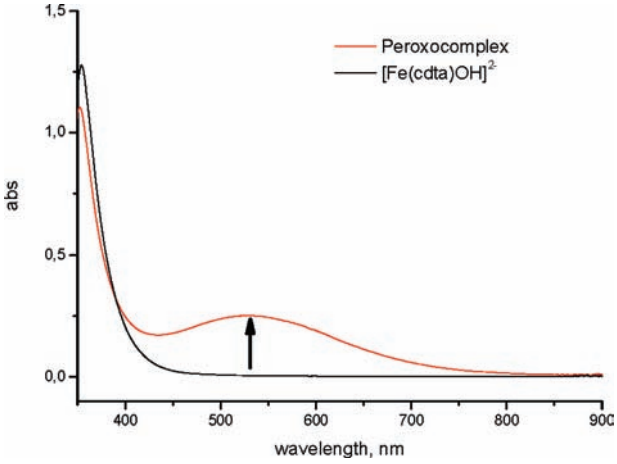

Figure 13. Spectral changes observed for the reaction of $[Fe^{III}(cydta)(H_2O)]^-$ with H_2O_2 at pH 10.9 (0.1 M glycine buffer). Experimental conditions: $[Fe(cydta)(H_2O)^-] = 0.001$ M, $[H_2O_2] = 0.01$ M, $I = 0.5$ M, $T = 25$ °C.

pK_a value of hydrogen peroxide the observed rate constant for the second reaction step of $[Fe(edta)(H_2O)]^-$ also shows a hydrogen peroxide concentration dependence. This suggests that OOH^- affects the second reaction step for both complexes (see further Discussion). The second reaction step can be assigned to an intramolecular rearrangement of an intermediate complex formed in the first reaction step as in the case of $[Fe(edta)(H_2O)]^-$. As a result of larger absorbance changes, the second reaction step was followed at 360 nm instead of at 545 nm used for the first reaction step. In analogy to $[Fe(edta)(H_2O)]^-$, the following reaction sequence is formulated for $[Fe(cydta)(H_2O)]^-$ as a working hypothesis.

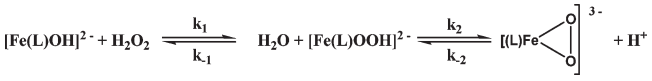

In the overall reaction, hydrogen peroxide binds reversibly to $[Fe(cydta)(H_2O)]^-$ to form an *end-on*-bound hydroperoxo complex, followed by a subsequent intramolecular rearrangement to a *side-on*-bound peroxo complex.

Kinetic Studies: Investigation of the First Reaction Step. The kinetics of this reaction was studied using stopped-flow spectroscopy. Kinetic data were obtained under pseudo-first-order conditions, $[H_2O_2] \gg [Fe(cydta)(H_2O)^-]$. As is known from earlier studies, the reaction of $[Fe(edta)(H_2O)]^-$ with hydrogen peroxide is sensitive to general acid catalysis.[14,16] To check if this also holds for $[Fe(cydta)(H_2O)]^-$, the effect of two different buffers on k_{1obs} was investigated. None of the employed buffers showed any interaction with the starting complex. The reaction was investigated in the pH range 10.25−11.0. Unless otherwise stated, the buffer concentration was 0.35 M throughout the measurements. The relatively limited pH range results, on the one hand, from the high reactivity of the complex and the dead time of the stopped-flow instrument and, on the other hand, from precipitation of iron hydroxide under such conditions. The dead time of the stopped-flow instrument is about 4 ms, and it was therefore not possible to measure below pH 10.25 because the reaction became too fast under such conditions. The addition of an equimolar concentration of H_4cydta could not prevent precipitation of iron hydroxide at pH > 11. In contrast, five different buffers could be employed in our earlier study on the $[Fe(edta)(H_2O)]^-$ system.

Kinetic traces measured in the presence of an excess of H_2O_2 showed a two-step behavior and could be fitted by a double-exponential function (see Figure 14). The time scale of the two steps was such that the overall reaction could be divided into two separate steps by selecting different time scales. It was then possible to fit each step to a single-exponential function. Plots of k_{1obs} versus the hydrogen peroxide concentration at different buffer concentrations showed to be linear with a significant intercept (Figure 15). The intercept was observed over the whole studied pH range. Although there is no significant change in the absorbance on going from the lowest to the highest hydrogen peroxide concentration, the intercept most likely represents a back-reaction, viz., decoordination of hydrogen peroxide. Because of the high k_{1obs} values, 1 half-life of the reaction lies within the dead time of the instrument. Therefore, it is even for the lowest buffer and hydrogen peroxide concentrations employed not possible to draw any conclusions from the magnitude of the absorbance changes. Plausibly, it can be concluded from the $[Fe(edta)(H_2O)]^-$ case that coordination of hydrogen peroxide is again a reversible process. The kinetic value of K ($=k_1/k_{-1}$) for pH 10.25 and 0.35 M buffers is 47.0 ± 0.3 M^{-1}. The rate law for the first reaction is given by eq 13.

$$k_{1obs} = k_1[H_2O_2] + k_{-1} \quad (13)$$

Again both the slope (k_1, forward reaction) and intercept (k_{-1}, back-reaction) are affected by general acid catalysis. To obtain more information on the buffer dependence, k_1 and k_{-1} were determined from similar plots, as in Figure 15, under various conditions and plotted against the concentration of the acidic form of the buffer, which is abbreviated as BH^+ in the remainder of the text. Plots of k_1 versus $[BH^+]$ at a fixed pH are linear with an intercept (Figure 16). Within the experimental error limits, the intercept is the same for all of the employed buffer concentrations and pH values. Only the data for glycine at pH 10.75 deviate slightly.

In contrast to $[Fe(edta)(H_2O)]^-$, where the intercepts of plots of k_1 versus $[BH^+]$ depend on the H^+ concentration, this is not observed in the case of $[Fe(cydta)(H_2O)]^-$. Straight lines at different pH values for the two buffers used show a common slope for the respective buffer and a common intercept for both buffers used, indicating that no additional $[H^+]$ dependence contributes to k_1. Most likely, the proton concentration in the investigated pH range is too low to have a significant affect on the rate of the reaction. The common intercept can be ascribed to the contribution of a spontaneous, non-acid-catalyzed reaction path. Equation 14 describes the various terms contributing to k_1, where k_{1BH} represents the general acid-catalyzed reaction and k_{H_2O} represents the spontaneous, non-acid-catalyzed path for the formation of

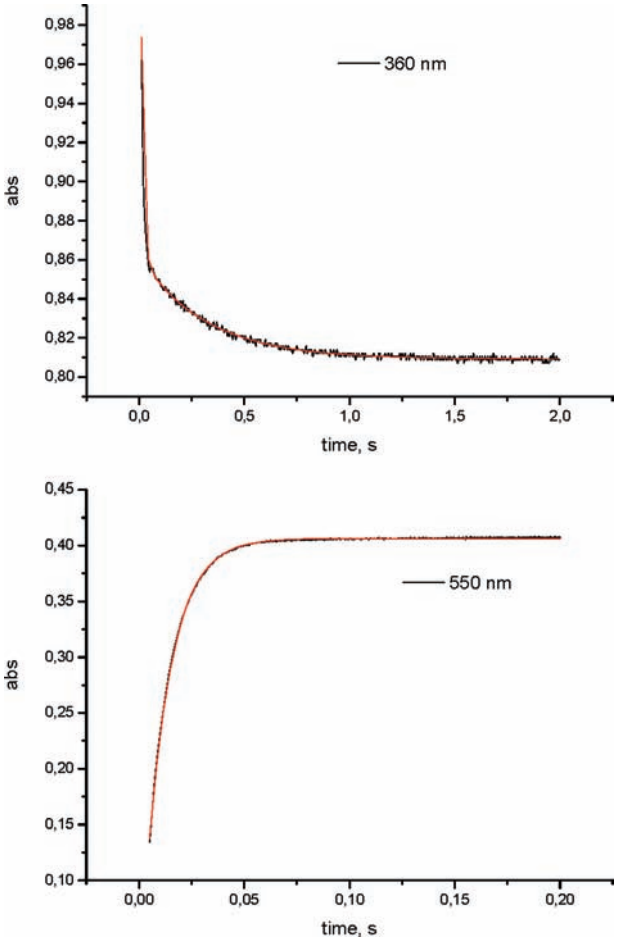

Figure 14. Typical kinetic traces at 360 nm (second reaction step) and 550 nm (first reaction step) observed for the reaction of $[Fe^{III}(cydta)(H_2O)]^-$ with H_2O_2 at pH 11.0 (0.35 M CAPS buffer). Experimental conditions: $[Fe(cydta)(H_2O)^-] = 0.001$ M, $[H_2O_2] = 0.01$ M, $I = 0.5$ M, $T = 25$ °C.

$[Fe(cydta)OOH]^{2-}$. k_{H_2O} can be determined from Figure 16 to be 4680 ± 280 M^{-1} s^{-1} at 25 °C.

$$k_1 = k_{1BH}[BH^+] + k_{H_2O} \quad (14)$$

The k_{1BH} values for glycine and CAPS correlate directly with the pK_a values of the two buffers. The lower the pK_a value, the stronger the acid and the higher the corresponding value for k_{1BH}. The effectiveness of general acid catalysis increases with a decrease in the pK_a value of the buffer. Upon comparison of the general acid contribution to k_1 for $[Fe(cydta)(H_2O)]^-$ and $[Fe(edta)(H_2O)]^-$, it is noteworthy that k_{1BH} for the respective buffer is about 1 order of magnitude (CAPS) and 2 orders of magnitude (glycine) larger for $[Fe(cydta)(H_2O)]^-$ than for $[Fe(edta)(H_2O)]^-$ (see Table 9).

Plots of k_{-1} versus $[BH^+]$ are linear with almost negligible intercepts. They can be described by eq 15, where the slope of the plots in Figure 17 represents the general acid-catalyzed back-reaction, k_{-1BH}. As in the case of $[Fe(edta)(H_2O)]^-$, the intercepts do not show a dependence on the H^+ concentration.

$$k_{-1} = k_{-1BH}[BH^+] \quad (15)$$

As in the case of $[Fe(edta)(H_2O)]^-$, the back-reaction is not catalyzed very effectively by glycine and CAPS. Because of their relatively low acid strength, they are not capable of enhancing the back-reaction very effectively. From a comparison of the absorbance changes observed at different pH values and the slopes of plots of $\log k_{1BH}$ versus pK_a, it can be concluded that in the case of $[Fe(edta)(H_2O)]^-$ the back-reaction was more affected by general acid catalysis than the forward reaction. As specified above, such a comparison of the absorbance changes is not possible for $[Fe(cydta)(H_2O)]^-$. The values of k_{-1BH} for CAPS buffer are of the same order of magnitude for $[Fe(cydta)(H_2O)]^-$ and $[Fe(edta)(H_2O)]^-$. From Figure 17, it can be concluded that, at low general acid concentrations up to about 0.08 M, k_{-1} values are only slightly affected by an increase in the general acid concentration (see the shaded part of Figure 17). This can be observed especially in the case of the glycine buffer at both investigated pH values. On going to general acid concentrations higher than 0.08 M, a significant increase in the values of k_{-1} is observed. A common observation for both studied systems is that formation of the hydroperoxo intermediate can only be observed at pH

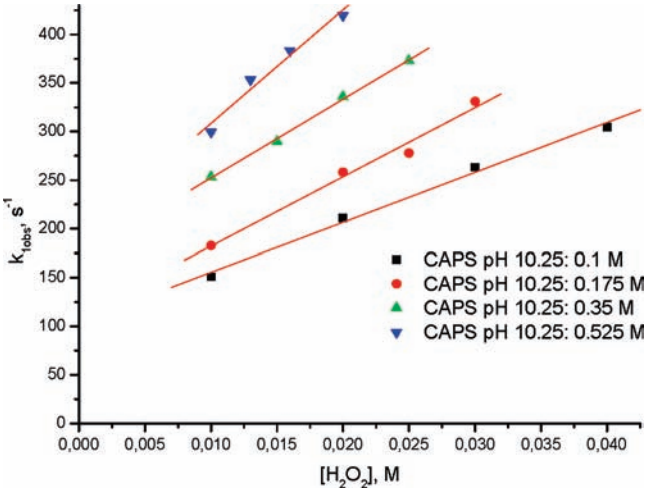

Figure 15. Plots of k_{1obs} versus $[H_2O_2]$ at pH 10.25 as a function of the CAPS buffer concentration. Experimental conditions: $[Fe(cydta)(H_2O)^-] = 0.001$ M, $I = 0.5$ M, $T = 25$ °C.

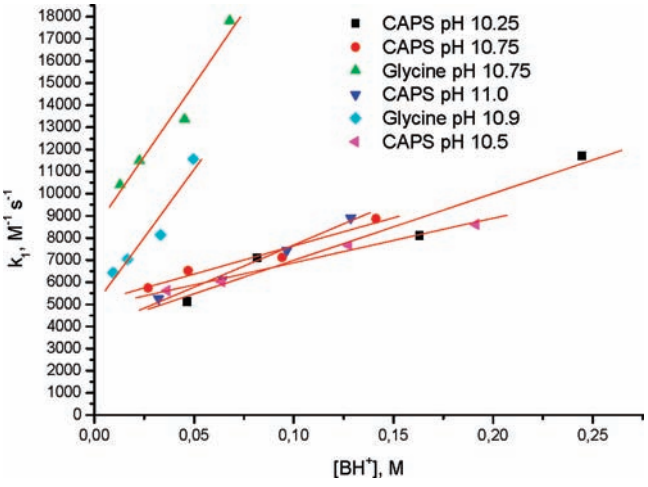

Figure 16. Plots of k_1 versus $[BH^+]$ for different buffers. Experimental conditions: $[Fe(cydta)(H_2O)^-] = 0.001$ M, $[H_2O_2] = 0.01 - 0.04$ M, $I = 0.5$ M, $T = 25$ °C.

Table 9. Summary of Rate Constants for the General Acid-Catalyzed Reaction Steps[a]

buffer	pK_a	k_{1BH}, $M^{-2}\,s^{-1}$	k_{-1BH}, $M^{-1}\,s^{-1}$	k_{-2BH}, $M^{-1}\,s^{-1}$
		[Fe(edta)(H_2O)]$^-$		
TAPS	8.4	$(2.8 \pm 0.1) \times 10^4$	$(1.0 \pm 0.1) \times 10^3$	
taurine	9.06	$(4.3 \pm 0.8) \times 10^4$	$(1.9 \pm 0.6) \times 10^3$	40 ± 2
AMPSO	9.1	$(1.3 \pm 0.1) \times 10^4$	$(0.4 \pm 0.1) \times 10^3$	
glycine	9.9	$(1.2 \pm 0.2) \times 10^3$	$(0.3 \pm 0.3) \times 10^3$	5.7 ± 0.6
CAPS	10.4	$(1.3 \pm 0.3) \times 10^3$	$(0.3 \pm 0.1) \times 10^3$	
		[Fe(cydta)(H_2O)]$^-$		
glycine	9.9	$(13 \pm 4) \times 10^4$		
CAPS	10.4	$(2.6 \pm 0.2) \times 10^4$	$(0.5 \pm 0.1) \times 10^3$	

[a] Experimental conditions: [Fe(cydta)(H_2O)$^-$] = [Fe(edta)(H_2O)$^-$] = 0.001 M, [H_2O_2] = 0.01−0.04 M, I = 0.5 M, T = 25 °C.

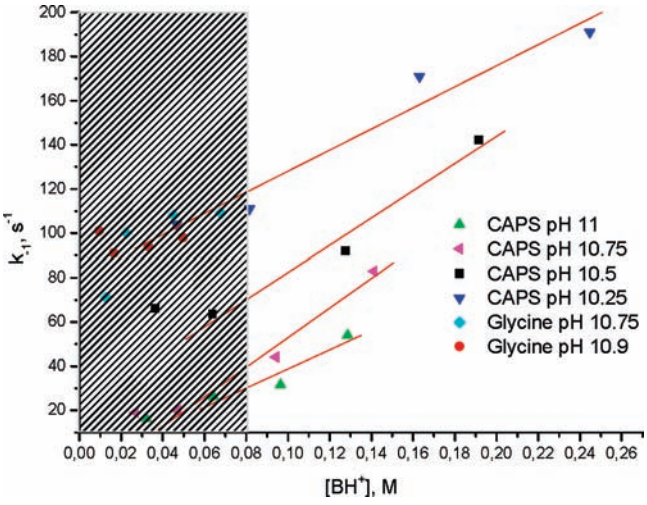

Figure 17. Plots of k_{-1} versus [BH^+] for different buffers. Experimental conditions: [Fe(cydta)(H_2O)$^-$] = 0.001 M, [H_2O_2] = 0.01−0.04 M, I = 0.5 M, T = 25 °C.

values higher than the pK_a value of [Fe(L)H_2O]$^-$. So, for both complexes, it is obvious that the pH of the solution controls the stability of the produced [Fe(L)OOH]$^{2-}$ complex (see the Results and Discussion section).

When all kinetic data reported above are combined, the observed overall rate constant for the first reaction step can be expressed by eq 16.

$$k_{1obs} = (k_{H_2O} + k_{1BH}[BH^+])[H_2O_2] + k_{-1BH}[BH^+] \quad (16)$$

For the complexes [Fe(edta)(H_2O)]$^-$[16] and [Fe(cydta)(H_2O)]$^-$, it was found that both forward and back reactions are affected by general acid catalysis. As in the case of [Fe(edta)(H_2O)]$^-$, the forward reaction can proceed via a spontaneous, non-acid-catalyzed reaction pathway, which could involve proton transfer from hydrogen peroxide to the [Fe(L)OH]$^-$ complex. In contrast to [Fe(edta)(H_2O)]$^-$, no evidence for an additional proton-catalyzed reaction pathway was found.

The reaction was also studied as a function of the temperature and pressure. Temperature and pressure dependences were studied at pH 11, where both forward and back reactions were observable. The effect of the temperature on the reaction of [Fe(cydta)(H_2O)]$^-$ with H_2O_2 was studied as a function of [H_2O_2] in a 0.1 M CAPS buffer over the range 4.7−30 °C. Eyring plots for k_1 and k_{-1} were constructed from the temperature dependence of k_{1obs} at pH 11.0 (see Figures S6 and S7 in the Supporting Information).

From these plots, the activation entropy, $\Delta S^{\ddagger}$, and the activation enthalpy, $\Delta H^{\ddagger}$, were determined. A reliable parameter for the mechanistic discrimination is the volume of activation, $\Delta V^{\ddagger} = RT(\mathrm{d} \ln k/\mathrm{d}P)_T$, where $\Delta V^{\ddagger}$ can be determined from the slope of a plot of ln k versus pressure. The effect of the pressure on the reaction of [Fe(cydta)(H_2O)]$^-$ with H_2O_2 was studied as a function of [H_2O_2] in a 0.1 M CAPS buffer at 0 °C over the pressure range 10−130 MPa (see Figure S8 in the Supporting Information).

From these data, the volume of activation for k_1 was determined. All activation parameters for the forward and back reactions at pH 11.0 are summarized in Table 10. To ensure that the absorbance changes for the first reaction step did not lie within the dead time of the high-pressure stopped-flow instrument, it was necessary to go to 0 °C in order to slow down the reaction significantly. At this temperature, the back-reaction could not be observed any more; thus, the volume of activation is only reported for the forward reaction.

Kinetic Studies: Investigation of the Second Reaction Step. The kinetics of this reaction was studied by stopped-flow spectroscopy in a CAPS buffer. It was also possible to observe a second reaction in a glycine buffer. The overall kinetic traces could be fitted to a double-exponential function by using different fitting routines, but the obtained k_{2obs} values were not constant for a single concentration. The absorbance changes for the second reaction step were much smaller than those for the first step, which complicated the fitting procedure. For that reason, only measurements in a CAPS buffer at pH 11.0, where good fits could be obtained, were taken into account. In the case of [Fe(edta)(H_2O)]$^-$, this reaction was found to be independent of the hydrogen peroxide concentration at pH 9.0 and 10.0. For [Fe(cydta)(H_2O)]$^-$, a weak dependence on the hydrogen peroxide concentration was observed at pH 11.0. A similar weak dependence was observed for [Fe(edta)(H_2O)]$^-$ when the reaction was remeasured at pH 11.0. Presumably, this reaction involves an intramolecular rearrangement to the [Fe^{III}(cydta)(η^2-O_2)]$^{3-}$ peroxo complex, which is catalyzed by OOH^- at pH values around the pK_a value of hydrogen peroxide. For Fe(edta), the [Fe^{III}(edta)(η^2-O_2)]$^{3-}$ peroxo complex has been well characterized.[6−9]

In contrast to [Fe(edta)(H_2O)]$^-$, where only sterically unhindered buffers like glycine and taurine that carry a primary amine function have a catalytic effect on the second reaction step, CAPS also affects the second reaction step of [Fe(cydta)(H_2O)]$^-$ with hydrogen peroxide (Figure 18). As is seen from this figure, only the intercept is affected by an increase in the buffer concentration. The slopes of the plots of k_{2obs} versus hydrogen peroxide concentration remain unaffected. In the Fe(edta) case, it could be concluded from the absorbance changes that k_{2obs} consists of two opposing reactions, viz., forward and back reactions. On the basis of mechanistic considerations, it was found that for Fe(edta) only the

Table 10. Summary of Rate Constants and Activation Parameters for the Two-Step Reaction[a]

	$[Fe(edta)(H_2O)]^-$			
	pH 9.0	pH 9.0	pH 10.5	pH 8.5
rate constant at 25 °C	$k_1 = 4000 \pm 141\ M^{-1}\ s^{-1}$	$k_{-1} = 145 \pm 4\ s^{-1}$	$k_{2obs} = 0.259 \pm 0.002\ s^{-1}$	$k_{-2obs} = 5.4 \pm 0.1\ s^{-1}$
$\Delta H^{\ddagger}$, kJ mol^{-1}	37 ± 4	101 ± 2	79 ± 2	86 ± 2
$\Delta S^{\ddagger}$, J K^{-1} mol^{-1}	-53 ± 14	$+135 \pm 6$	-10 ± 5	$+56 \pm 6$
$\Delta V^{\ddagger}$, cm^3 mol^{-1}	$+6.8 \pm 0.8$	$+18.4 \pm 0.6$	-2.3 ± 0.1	$+5.1 \pm 0.2$
	$[Fe(cydta)(H_2O)]^-$			
	pH 11.0	pH 11.0	pH 11.0	pH 11.0
rate constant at 25 °C	$k_1 = 6129 \pm 467\ M^{-1}\ s^{-1}$	$k_{-1} = 26 \pm 13\ s^{-1}$	$k_2 = 2.78 \pm 0.05\ s^{-1}$	$k_2^* = 33 \pm 2\ M^{-1}\ s^{-1}$
$\Delta H^{\ddagger}$, kJ mol^{-1}	41 ± 3	109 ± 5	55 ± 3	52 ± 2
$\Delta S^{\ddagger}$, J K^{-1} mol^{-1}	-37 ± 10	$+142 \pm 18$	-33 ± 11	-61 ± 5
$\Delta V^{\ddagger}$, cm^3 mol^{-1}	$+6 \pm 1$		-12 ± 2	-9 ± 2

[a] Experimental conditions: $[Fe(edta)(H_2O)^-] = [Fe(cydta)(H_2O)^-] = 0.001$ M, $[H_2O_2] = 0.01-0.04$ M, $I = 0.5$ M, $T = 25$ °C.

back-reaction is affected by general acid catalysis. For Fe(edta), there was no back-reaction observed above pH 10 in glycine and CAPS buffers. In the case of Fe(cydta), where measurements could only be performed at pH 11, no back-reaction was observed at all. The intercepts in Figure 18 do not represent a back-reaction but a buffer-catalyzed parallel reaction, also leading to the side-on-bound peroxo complex. Taking into account that only the forward reaction, viz., deprotonation of the hydroperoxo complex, that leads to the side-on peroxo complex is affected by an increase in the buffer concentration, it can be concluded that $[BH^+]$ cannot play a role in this reaction. Presumably, the buffer anion $[B^-]$ assists deprotonation of the hydroperoxo complex. For glycine buffers, this effect should play a secondary role because, due to its lower pK_a value, the buffer anion of glycine should be less basic than that of CAPS. Most likely, deprotonated hydrogen peroxide acts in a way similar to that of the buffer anion. It assists the deprotonation of the *end-on* hydroperoxo complex. The observed rate constant for the second step of the reaction can be expressed by eq 17:

$$k_{2obs} = k_2[B^-] + k_2^*[OOH^-] \qquad (17)$$

The influence of the temperature and pressure on this reaction was studied. Kinetic data for temperature and pressure dependences were measured at pH 11 in a CAPS buffer. The temperature dependence of k_{2obs} as a function of $[H_2O_2]$ at pH 11.0 (see Figure S9 in the Supporting Information) was used to construct linear Eyring plots for k_2 and k_2^*, from which $\Delta S^{\ddagger}$ and $\Delta H^{\ddagger}$ were determined (see Figures S10 and S11 in the Supporting Information). The effect of the pressure on k_{2obs} was investigated as a function of $[H_2O_2]$ at pH 11.0 and 25 °C over the pressure range 10−130 MPa (see Figure S12 in the Supporting Information). From these data, the volumes of activation for k_2 and k_2^* were determined (see Figures S13 and S14, in the Supporting Information). It turned out that all obtained activation parameters for k_2 and k_2^* were very similar at pH 11.0, viz., $\Delta S^{\ddagger} = -33 \pm 11$ J K^{-1} mol^{-1}, $\Delta H^{\ddagger} = 55 \pm 3$ kJ mol^{-1}, $\Delta V^{\ddagger} = 12 \pm 2$ cm^3 mol^{-1} for k_2 and $\Delta S^{\ddagger} = -61 \pm 5$ J K^{-1} mol^{-1}, $\Delta H^{\ddagger} = 52 \pm 2$ kJ mol^{-1}, $\Delta V^{\ddagger} = 9 \pm 2$ cm^3 mol^{-1} for k_2^*, indicating that both reactions lead to the same end product only via different pathways. All activation parameters are summarized in Table 10. The reported activation volume for k_1 ($\Delta V^{\ddagger} = +6 \pm 1$ cm^3 mol^{-1}) points to an I_d mechanism for the ligand substitution reaction on $[Fe(cydta)OH_2]^-$ by hydrogen peroxide and follows the same mechanism as the water-exchange reaction on $[Fe^{III}(cydta)(H_2O)]^-$. For the back-reaction, a very large and positive $\Delta S^{\ddagger}$ is observed, suggesting a stronger dissociative character. For the second reaction step, negative $\Delta S^{\ddagger}$ (-33 ± 11 J K^{-1} mol^{-1}) and $\Delta V^{\ddagger}$ (-12 ± 2 cm^3 mol^{-1}) were found for the intramolecular rearrangement, which is in agreement with an I_a type of mechanism for the peroxide chelation reaction. For the second reaction step, no back-reaction could be observed.

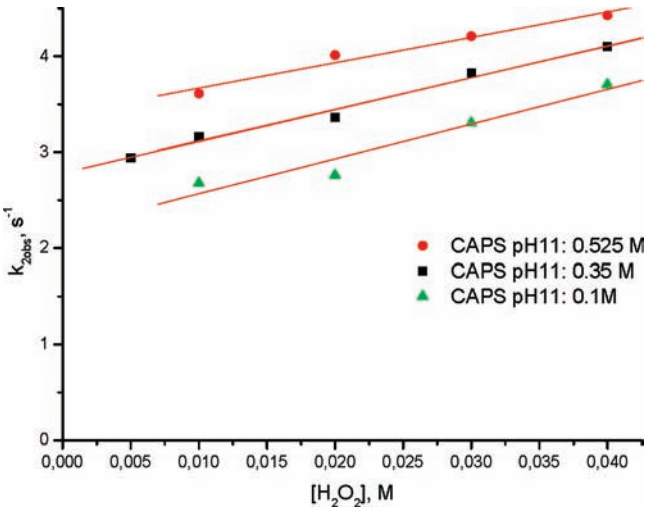

Figure 18. Plots of k_{2obs} versus $[H_2O_2]$ at pH 11.0 (CAPS) as a function of the buffer concentration. Experimental conditions: $[Fe(cydta)(H_2O)^-] = 0.001$ M, $I = 0.5$ M, $T = 25$ °C.

Mechanistic Considerations. Scheme 4 shows the suggested mechanism for the overall reaction based on the obtained data. As in the case of $[Fe(edta)]^-$, the reaction of $[Fe(cydta)]^-$ with hydrogen peroxide resulting in the violet $[Fe^{III}(cydta)(\eta^2\text{-}O_2)]^{3-}$ peroxo complex is only observable at pH values significantly larger than the pK_a of $[Fe(cydta)H_2O]^-$. The pK_a value of $[Fe(cydta)H_2O]^-$, which consists of three consecutive reactions involving aquation, deprotonation, and ring opening, has, because

of a much smaller equilibrium constant for the ring-opening reaction, a value of 9.54, i.e., two units above the pK_a value of $[Fe(edta)H_2O]^-$. Both methods, viz., pH-dependent spectrophotometric titration and Mössbauer measurements, suggest that under the employed conditions the main reacting species in solution is a seven-coordinate Fe(hydroxo) complex $[Fe(cydta)OH]^{2-}$. Dimer formation, which is less favored for Fe(cydta) than for Fe(edta), does not play an important role in this concentration range. This can actually be seen in the Mössbauer spectrum at pH 10.4, where even at a high total iron concentration both the monomer $[Fe(cydta)H_2O]^-$ and dimer $[\{Fe(cydta)\}_2(\mu\text{-}O)]^{4-}$ coexist in solution.

$[Fe(cydta)OH]^{2-}$ itself is nonreactive, but it can be protonated either by H^+ ions or by the acidic form of the buffer BH^+. This protonation results in the more labile aqua species $[Fe(cydta)H_2O]^-$, which reacts rapidly with hydrogen peroxide to give $[Fe^{III}(cydta)(\eta^2\text{-}O_2)]^{3-}$. In the case of Fe(cydta), the H^+ concentration is very low as compared to the BH^+ concentration, and only general acid catalysis is evident. Protonation of $[Fe(cydta)OH]^{2-}$ to form $[Fe(cydta)H_2O]^-$ involves charge neutralization and therefore may give a small positive contribution to $\Delta V^{\ddagger}$. For the water-exchange reaction on $[Fe(cydta)H_2O]^-$, a volume of activation of $+2.3 \pm 0.1$ cm^3 mol^{-1} was measured, suggesting a dissociative interchange (I_d) mechanism. Taking into account an additional positive contribution to the volume of activation due to charge neutralization, one finds that this is in close agreement with the observed volume of activation for k_1, viz., 6 ± 1 cm^3 mol^{-1} at pH 11. Thus, the reaction of $[Fe(cydta)H_2O]^-$ with H_2O_2 follows, parallel to $[Fe(edta)H_2O]^-$, an I_d mechanism characterized by a small positive $\Delta V^{\ddagger}$, as found for the water exchange on $[Fe(cydta)H_2O]^-$. There are two possible pathways for the first reaction step to occur, either a general acid-catalyzed pathway involving protonation of $[Fe(cydta)OH]^{2-}$ by the acid form of the buffer or a spontaneous pathway where H_2O_2 acts as the protonating species. In the latter case, H_2O_2 directly attacks $[Fe(cydta)OH]^{2-}$ to form the labile aqua species.

As was already discussed for $[Fe(edta)(H_2O_2)]^-$, because of an electron-withdrawing effect of the positively charged metal center, the pK_a value for coordinated hydrogen peroxide will be a few units lower than that for free H_2O_2. For $[Fe(edta)(H_2O_2)]^-$, the pK_a value for coordinated hydrogen peroxide was estimated to be 7.6,[16] thus in the range of the pK_a value of $[Fe(edta)H_2O]^-$. Apparently, this also holds for $[Fe(cydta)H_2O]^-$. The reaction only takes place at pH values above the pK_a of the complex, so it can be assumed that the pK_a value of the coordinated hydrogen peroxide in $[Fe(cydta)(H_2O_2)]^-$ lies around 9.5. Possibly, the pK_a value for coordinated H_2O_2 is also a composite value of three different equilibrium constants, similar to the pK_a value of the $[Fe(L)(H_2O)]^-$ aqua complexes. Thus, the same explanation could account for the pK_a values of coordinated H_2O_2 in $[Fe(edta)(H_2O_2)]^-$ and $[Fe(cydta)(H_2O_2)]^-$ to also differ by two units. Because of this pK_a value, $[Fe(cydta)(H_2O_2)]^-$ can be stabilized by deprotonation to give the $[Fe(cydta)(OOH)]^{2-}$ *end-on*-bound hydroperoxo complex at high pH values.

Scheme 4. Suggested Mechanism for the Overall Reaction of $[Fe(cydta)]^-$ with H_2O_2 in a Buffered Solution

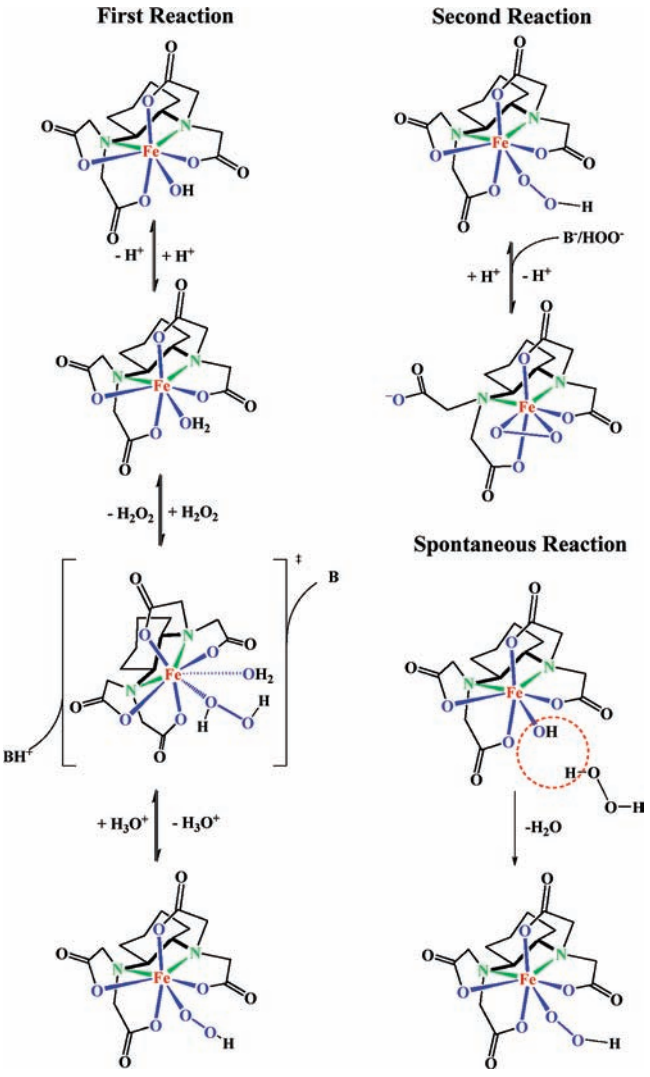

As in the case of Fe^{III}edta, the back-reaction, viz., the protonation of the $[Fe(cydta)(OOH)]^{2-}$ hydroperoxo complex is also sensitive to general acid catalysis. The acidic form of the buffer protonates the $[Fe(cydta)(OOH)]^{2-}$ complex, and hydrogen peroxide dissociates. The acid strength of the protonated form of CAPS and glycine is not high enough to catalyze the back-reaction very efficiently, but a small effect can be observed. The observed entropy of activation, viz., $\Delta S^{\ddagger} = +142 \pm 18$ J K^{-1} mol^{-1}, indicates that the reaction follows a dissociative D mechanism. A striking similarity in the activation parameters for k_1 and k_{-1} for Fe(edta) and Fe(cydta) is observed. Obviously, the same mechanism for the coordination of hydrogen peroxide holds in both cases (see Table 10).

The overall reaction cannot be observed at low pH values because of the inability of the hydrogen peroxide complex $[Fe^{III}(cydta)(H_2O_2)]^-$ to stabilize itself by deprotonation because of the higher H^+ concentration. H_2O_2 has to compete with a large excess of water to coordinate to the iron center, and decomposition of $[Fe^{III}(cydta)(H_2O_2)]^-$ is the immediate consequence.

After formation of the *end-on*-bound hydroperoxo complex, a slower second step can be observed.

In the case of Fe(edta), this second step was at pH values up to ca. 10, the $[H_2O_2]$-independent intramolecular rearrangement to a seven-coordinate $[Fe^{III}(edta)(\eta^2\text{-}O_2)]^{3-}$ peroxo complex. The forward reaction follows an associative interchange (I_a) mechanism characterized by small negative volume and entropy of activation values (see Table 10). The back-reaction for Fe(edta) follows a dissociative interchange mechanism (I_d) with small positive volume and entropy of activation values (see Table 10). The back-reaction is affected by general acid catalysis. The acidic form of sterically unhindered buffers protonates the $[Fe^{III}(edta)(\eta^2\text{-}O_2)]^{3-}$ complex.

For Fe(cydta), the situation is different. Indeed, the reaction product is of the same type as that for Fe(edta), viz., $[Fe^{III}(cydta)(\eta^2\text{-}O_2)]^{3-}$, characterized in this study to be the seven-coordinate *side-on*-bound peroxo complex with one chelate arm detached. However, the reaction pathway is slightly different. No back-reaction could be observed at pH 11. The *side-on*-bound peroxo complex $[Fe^{III}(cydta)(\eta^2\text{-}O_2)]^{3-}$ is reached via an I_a mechanism with negative values for the volume and entropy of activation. There are two possible pathways to reach the *side-on*-bound peroxo complex. One is base-catalyzed, and the second one is catalyzed by deprotonated hydrogen peroxide, OOH^-. The obtained activation parameters for the different pathways are $\Delta S^{\ddagger} = -33 \pm 11\ J\ K^{-1}\ mol^{-1}$, $\Delta V^{\ddagger} = -12 \pm 2\ cm^3\ mol^{-1}$ and $\Delta S^{\ddagger} = -61 \pm 5\ J\ K^{-1}\ mol^{-1}$, $\Delta V^{\ddagger} = -9 \pm 2\ cm^3\ mol^{-1}$, respectively. It is known from spectrophotometric titrations performed in this study that for Fe(edta) ring opening (detachment of a carboxylate arm) is more favored compared to that for Fe(cydta). For Fe(edta), a seven-coordinate *side-on* peroxo complex with one carboxylate arm detached was proposed. The detachment should occur during formation of the *side-on* peroxo complex to avoid the formation of an eight-coordinate iron(III) complex. This process can be visualized as an interchange reaction, during which coordinated peroxide goes from *end-on* to *side-on* accompanied by the dechelation of a carboxylate arm. Entropy and volume changes are expected to arise from intrinsic volume changes associated with the *end-on* to *side-on* change in bonding mode and dechelation of a carboxylate arm. In addition, dechelation also leads to charge creation and an increase in electrostriction, i.e., a decrease in the volume and entropy, as a result of the influence of the negative charge on the carboxylate group on the surrounding solvent molecules. The reported $\Delta S^{\ddagger}$ and $\Delta V^{\ddagger}$ values suggest that the interchange process has an associative character (I_a) in terms of the sign and magnitude of these values. For Fe(cydta), negative values for $\Delta S^{\ddagger}$ and $\Delta V^{\ddagger}$ were also reported, therefore also pointing to an interchange process with an associative character.

As was already mentioned above, there are two possible pathways for the second reaction step. The first pathway is again affected by the buffer concentration, but in this case, general base catalysis is evident, where the buffer anion deprotonates the hydroperoxo complex to give the $[Fe^{III}(edta)(\eta^2\text{-}O_2)]^{3-}$ complex. The second pathway is influenced by the H_2O_2 concentration. At pH values around the pK_a of hydrogen peroxide ($pK_a = 11.6$) where H_2O_2 is partly deprotonated, OOH^- can act as a deprotonating agent, leading to the *side-on*-bound peroxo complex. After reinvestigation of the rearrangement reaction for Fe(edta) at pH 11, this small effect was also observed. It is not straightforward to explain the different behavior of the respective hydroperoxo complexes of edta and cydta toward the buffer concentration. Possibly there are small changes in the structure of the hydroperoxo complexes, leading to an altered cavity for the buffer to attack.

For both the complexes Fe(edta) and Fe(cydta), no evidence for the formation of high-valent iron oxo species in the presence of hydrogen peroxide was found. It is known from the literature that six-coordinate iron(III) hydroperoxo complexes are activated toward homolytic cleavage of the O−O bond. A strong σ-donor interaction strengthens the Fe−O bond, which is accompanied by a weakening of the O−O bond and the formation of high-valent iron oxo species. Because of a different electronic structure, this order is reversed in high-spin iron(III) hydroperoxo complexes. The different electronic situation is also reflected in a higher energy barrier for the homolytic cleavage of the O−O bond.[76,77] In the cases of Fe(edta) and Fe(cydta), high-spin peroxo complexes are formed.

Catalysts that support high oxidation states of iron are often based on N-donor ligands.[78] In contrast, edta and cydta have mainly O-donor functions, which give rise to a small ligand-field splitting compared to N-donor ligands and the formation of high-spin complexes. It is likely that this change in the ligand donor ability alters the electronic situation in the formed high-spin peroxo complexes such that O−O bond splitting becomes unfavorable. It is also known from the literature[79] that deprotonation of a low-spin Fe^{III}−OOH complex with NEt_3 in methanol leads to a high-spin iron(III) peroxo complex, which is less reactive to cleavage of the O−O bond compared to the low-spin Fe^{III}−OOH complex.

Conclusions

In this study, the complete speciation of $[Fe^{III}(L)H_2O]^-$ (L = edta, cydta, and pdta) in water was presented and an explanation for the difference in the pK_a values for $[Fe^{III}(edta)(H_2O)]^-$ and $[Fe^{III}(cydta)H_2O]^-$ was offered. Analogous to $[Fe^{III}(edta)H_2O]^-$, the reactivity of $[Fe^{III}(cydta)H_2O]^-$ toward hydrogen peroxide was investigated and a reaction mechanism for the two-step reaction was presented. Although the main reaction pathway is similar to that for $[Fe^{III}(edta)H_2O]^-$, small differences were observed. It turned out once again that small changes in the reaction conditions can influence the reactivity significantly. In both cases with edta and cydta as chelates for Fe^{III}, it was shown that buffer catalysis has a significant influence on the reaction rate. The final product of the reaction is of the same type for both

(76) Lehnert, N.; Ho, R. Y. N.; Que, L.; Solomon, E. I. *J. Am. Chem. Soc.* **2001**, *123*, 12802–12816.
(77) Solomon, E. I.; Wong, S. D.; Liu, L. V.; Decker, A.; Chow, M. S. *Curr. Opin. Chem. Biol.* **2009**, *13*, 99–113.
(78) Kryatov, S. V.; Rybak-Akimova, E. V.; Schindler, S. *Chem. Rev.* **2005**, *105*, 2175–2226.
(79) Jensen, K. B.; McKenzie, C. J.; Nielsen, L. P.; Pedersen, J. Z.; Svendsen, H. M. *Chem. Commun.* **1999**, 1313–1314.

chelates, viz., a seven-coordinate $[Fe^{III}(L)(\eta^2\text{-}O_2)]^{3-}$ complex. The structure of the $[Fe^{III}(cydta)(\eta^2\text{-}O_2)]^{3-}$ complex was clarified with Mössbauer spectroscopy. The reaction mechanism for the first reaction is exactly the same for both chelates and follows a dissociative interchange mechanism for both the forward and back reactions. The reactivity is controlled by the substitution behavior of $[Fe^{III}(L)H_2O]^-$. The rate and activation parameters for water exchange on $[Fe^{III}(cydta)H_2O]^-$ were remeasured. The *end-on*-coordinated hydroperoxo complex generated in the first reaction step reacts further in an associative interchange manner to form the $[Fe^{III}(L)(\eta^2\text{-}O_2)]^{3-}$ peroxo complex. Although the resulting peroxo complex is similar in both cases, the buffer plays a different role. For Fe(edta), the buffer cation catalyzes the back-reaction, viz., ring opening of the peroxo complex, whereas for Fe(cydta), the buffer anion catalyzes the chelation of the coordinated peroxide from *end-on* to *side-on*. The reason for this difference is not clear. We hope that ongoing density functional theory calculations will offer a possible explanation for this difference.

Acknowledgment. The authors gratefully acknowledge financial support from the Deutsche Forschungsgemeinschaft (DFG) through Grants SFB 583, SPP 1118, and ME 1148/7-1, as well as from the Hungarian National Science Fund (OTKA) and National Agency for Research and Technology (NKTH) (Grant K-67835).

Supporting Information Available: Additional information on the structure of $K[Fe(cydta)(H_2O)]\cdot 3H_2O$, technical details for the pH-dependent spectrophotometric titration of $[Fe^{III}(cydta)(H_2O)]^-$, details and background of the Mössbauer measurements, additional figures to illustrate the evaluation of the kinetic data and the activation parameters, and data treatment for the pressure- and temperature-dependent ^{17}O NMR measurements. This material is available free of charge via the Internet at http://pubs.acs.org.